Force and phosphate release from Arp2/3 complex promote dissociation of actin filament branches

Nandan G. Pandit[a,b], Wenxiang Cao[a], Jeffrey Bibeau[a], Eric M. Johnson-Chavarria[a], Edwin W. Taylor[a], Thomas D. Pollard[a,b,c,d], and Enrique M. De La Cruz[a,b,1]

[a]Department of Molecular Biophysics and Biochemistry, Yale University, New Haven, CT 06520; [b]Program in Physical and Engineering Biology, Yale University, New Haven, CT 06520; [c]Department of Molecular, Cellular, and Developmental Biology, Yale University, New Haven, CT 06520; and [d]Department of Cell Biology, Yale University, New Haven, CT 06520

Edited by Harry Higgs, Geisel School of Medicine at Dartmouth, Hanover, NH, and accepted by Editorial Board Member Yale E. Goldman April 16, 2020 (received for review June 28, 2019)

Networks of branched actin filaments formed by Arp2/3 complex generate and experience mechanical forces during essential cellular functions, including cell motility and endocytosis. External forces regulate the assembly and architecture of branched actin networks both in vitro and in cells. Considerably less is known about how mechanical forces influence the disassembly of actin filament networks, specifically, the dissociation of branches. We used microfluidics to apply force to branches formed from purified muscle actin and fission yeast Arp2/3 complex and observed debranching events in real time with total internal reflection fluorescence microscopy. Low forces in the range of 0 pN to 2 pN on branches accelerated their dissociation from mother filaments more than two orders of magnitude, from hours to <1 min. Neither force on the mother filament nor thermal fluctuations in mother filament shape influenced debranching. Arp2/3 complex at branch junctions adopts two distinct mechanical states with different sensitivities to force, which we name "young/strong" and "old/weak." The "young/strong" state 1 has adenosine 5′-diphosphate (ADP)–P_i bound to Arp2/3 complex. Phosphate release converts Arp2/3 complex into the "old/weak" state 2 with bound ADP, which is 20 times more sensitive to force than state 1. Branches with ADP–Arp2/3 complex are more sensitive to debranching by fission yeast GMF (glia maturation factor) than branches with ADP–P_i–Arp2/3 complex. These findings suggest that aging of branch junctions by phosphate release from Arp2/3 complex and mechanical forces contribute to disassembling "old" actin filament branches in cells.

actin | Arp2/3 complex | branched filament | debranching | force

Arp2/3 complex forms networks of branched actin filaments that generate and sustain mechanical forces that power cell motility, endocytosis, and vesicle trafficking (1, 2). Membrane-bound proteins, called nucleation-promoting factors, such as WASP activate Arp2/3 complex, which then nucleates a branch when it binds to the side of a preexisting "mother" filament (3). The new "daughter" filament elongates and pushes against the membrane until it is capped. All of the filaments, including branches formed by Arp2/3 complex, must disassemble for recycling to form new filaments and branches. Similar to actin, Arp2/3 complex is an ATPase (4–6). Hydrolysis of bound ATP and subsequent phosphate release have been implicated in controlling branched network dynamics (5, 7–10), but mechanistic details are lacking.

The assembly and architecture of branched actin networks are sensitive to force in vitro and in cells (11, 12). Under load, branched actin networks assembled from purified proteins grow more slowly and with a higher branch density (13, 14), but how these mechanical forces directly affect the biochemical interactions of branched actin network protein components has not been firmly established. Similar to measurements with purified protein components, branched actin networks in cells respond to external load by increasing density of branched filaments while also reorganizing relative to the membrane (15).

Networks of branched actin filaments turn over much more rapidly in cells than in vitro when assembled from purified proteins (16–19). The regulatory proteins cofilin and glia maturation factor (GMF) accelerate debranching and have been implicated in accelerating branched network remodeling and turnover (20–24). Although not investigated previously, mechanical forces may also affect network disassembly through debranching.

We report that mechanical forces promote dissociation of branches formed by Arp2/3 complex and that phosphate bound to Arp2/3 complex regulates the sensitivity to force. Phosphate release from Arp 2/3 complex at branch junctions also regulates debranching by GMF. Thus, phosphate release from the Arp2/3 complex could target "older" adenosine 5′-diphosphate (ADP)–Arp2/3 branches for dissociation while sparing "younger" branches with ADP–P_i–Arp2/3 complex.

Results

Microfluidics Assay to Measure Dissociation of Branches Formed by Arp2/3 Complex under Force. We used fluid flowing through a microfluidics apparatus to apply force to actin filament branches formed by purified fission yeast Arp2/3 complex and muscle actin monomers (Fig. 1*A*) as we observed the dissociation of the branches by fluorescence microscopy. Starting with short filament seeds tethered to the surface of the slide, we assembled branched filaments from purified ATP-actin monomers and

Significance

Arp2/3 complex is an ATPase that binds to the side of a preexisting actin filament and nucleates an actin filament branch. Growing branched networks experience variable resistance and respond by adapting growth speed, power, and architecture. How force influences the dissociation of actin filament branches was not known. We used microfluidics to show that mechanical force promotes the dissociation of actin filament branches and that Arp2/3 complex adopts two distinct mechanical states with different responses to force. Phosphate release from Arp2/3 complex increases the sensitivity to both force and the debranching protein GMF. Thus, phosphate release from Arp2/3 complex may regulate debranching by force and debranching proteins.

Author contributions: N.G.P. and E.M.D.L.C. designed research; N.G.P. performed research; N.G.P., W.C., J.B., E.M.J.-C., E.W.T., T.D.P., and E.M.D.L.C. contributed new reagents/analytic tools; N.G.P., W.C., J.B., E.W.T., T.D.P., and E.M.D.L.C. analyzed data; and N.G.P., W.C., J.B., E.W.T., T.D.P., and E.M.D.L.C. wrote the paper.

The authors declare no competing interest.

This article is a PNAS Direct Submission. H.H. is a guest editor invited by the Editorial Board.

[1]To whom correspondence may be addressed. Email: enrique.delacruz@yale.edu.

This article contains supporting information online at https://www.pnas.org/lookup/suppl/doi:10.1073/pnas.1911183117/-/DCSupplemental.

First published May 27, 2020.

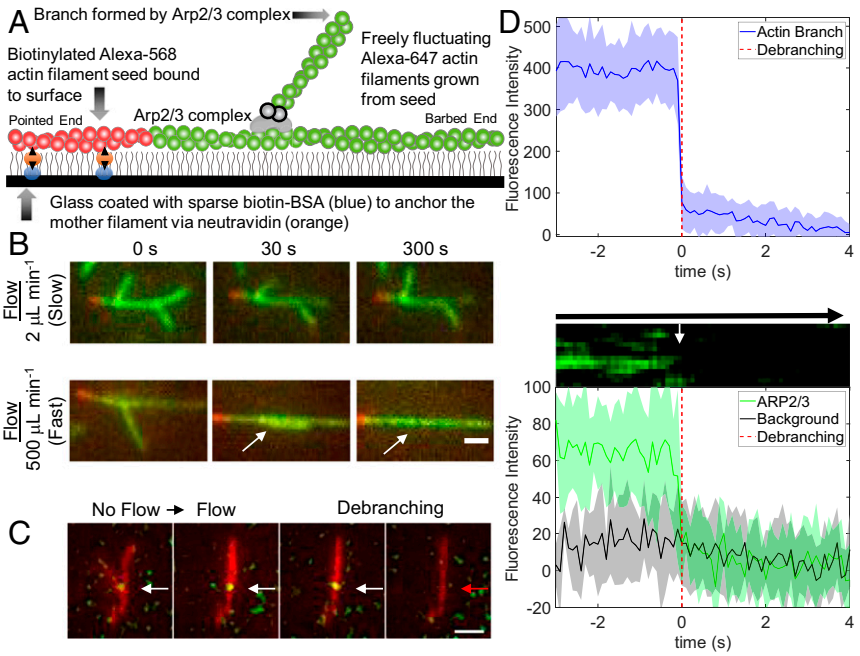

Fig. 1. Microfluidics assay to measure Arp2/3 complex debranching under force. (*A*) Diagram showing a short segment of an actin filament containing 10% biotinylated and 15% Alexa 568-labeled (red) actin subunits immobilized on the neutravidin-coated surface. The surface is passivated with 0.2% tween (illustrated with gray vertical lines). This seed was elongated at its barbed end with 1.5 μM 15% Alexa 647-labeled Mg-ATP-actin (green), and Arp2/3 complex formed a branch with Alexa 647-labeled Mg-ATP-actin. The green filaments fluctuate freely and are subject to viscous drag forces applied by fluid flow. (*B*) TIRF microscopy images of representative branched filaments under slow flow (2 μL·min^{-1}, ~0.004 pN of force for a 1.5-μm branch; *Top*) and fast flow (500 μL·min^{-1}, ~1.02 pN of force for a 1.5-μm branch; *Bottom*). Branches are aligned in the direction of flow. (Scale bar, 1 μm.) (*C*) The Arpc5 subunit of the Arp2/3 complex was labeled with Alexa 488 via snap tag and tracked during debranching. Time-lapse images with the actin filaments represented in red and the Alexa 488–Arp2/3 complex located at the junction of the daughter branch and mother filament represented in green. (Scale bar, 1 μm.) (*D*) *Top* shows the spatially integrated fluorescence intensity of actin at a branch junction as a function of time, used to determine the observed debranching event time ($t = 0$). *Middle* shows a kymograph measured across a branched actin filament. *Bottom* shows the time course of spatially integrated fluorescence intensity of Arpc5 subunit at a branch junction with time aligned to its corresponding actin frame. The fluorescence intensity from Arp2/3 complex reproducibly decreased in a single step for all 12 debranching events observed.

Arp2/3 complex for 2 min to 4 min. After washing out the soluble proteins, the filaments were allowed to "age" for an additional, variable time with very slow fluid flow. Thereafter, we started the debranching process under constant force by flowing buffer over the surface at a rate of 2 μL·min^{-1} to 500 μL·min^{-1} until the end of the experiment, while we recorded a series of images. The seeds were immobilized on the slide, but both the mother filaments and branches were free to fluctuate (Fig. 1*A*).

Rapid flow rates flattened branches against the mother filaments until they dissociated (Fig. 1*B* and Movies S1–S3). Neither the angle of the applied force (relative to mother filament orientation), the tension in the mother filament, nor fluctuations in mother filament shape had a strong influence on debranching (*SI Appendix*, Fig. S1 and Movies S6 and S7).

We added a snap tag to the Arpc5 subunit of Arp2/3 complex for labeling with Alexa 488 and simultaneous viewing with Alexa 647-labeled actin. Force dissociated Arp2/3 complex and the daughter filament concurrently, within the 0.1-s time resolution of our imaging (Fig. 1*D* and Movies S4 and S5). Buffer flowed across the sample at 500 μm·s^{-1} dissociated both the daughter filament and Arp2/3 complex from the field of view by the next frame, making it impossible to determine whether the labeled Arp2/3 complex remained bound to the dissociated daughter filament.

Piconewton Forces Decreased the Time for Branch Dissociation from Hours to <1 Min. Branches formed by ATP–Arp2/3 complex were stable for many minutes without buffer flow (Fig. 2*A*) but had a higher probability of dissociating when subjected to the forces produced by the range of buffer flow rates in our experiments (Fig. 2*A*). The following sections explain how the time course of debranching depends on the applied force and how long the newly formed branches were aged after assembly. At a given flow rate, the force on a branch scales with its length. In some experiments, we show the force on individual branches (*SI Appendix*, Fig. S2), but, in most experiments, we report flow rates from which we calculate the average force on branches (e.g., Fig. 2*A*).

In samples of branches formed by ATP–Arp2/3 complex and aged for 30 min, the time course of debranching followed a single exponential that depended on the applied force (Fig. 2*A*). The observed lifetimes of these branches decreased with force (Fig. 2*D*), suggesting a slip bond behavior, so we used the Bell's equation (25) (Eq. **1**) to estimate the force sensitivity,

$$\tau_{obs} = \tau_0 e^{-\frac{Fd}{k_B T}}. \quad [1]$$

Here k_B is the Boltzmann constant, T is the absolute temperature, F is force, τ_0 is the branch lifetime in the absence of force, and d is the characteristic distance to the transition state (26). The value of d is typically considered a force sensitivity parameter for bond rupture. An alternative estimate of force dependence is the force that reduces the branch lifetime by half (half-force, $F_{1/2} = 0.693 k_B T/d$), which we estimate to be 0.054 (±0.008) pN.

Without force, the branch lifetime (τ_0), estimated from extrapolation of the fit of the force dependence (Fig. 2*D*), was 106 (±8) min [Table 1; $k_2 \approx 1/\tau_0 = 0.01$ (±0.0007) min^{-1}], indicating

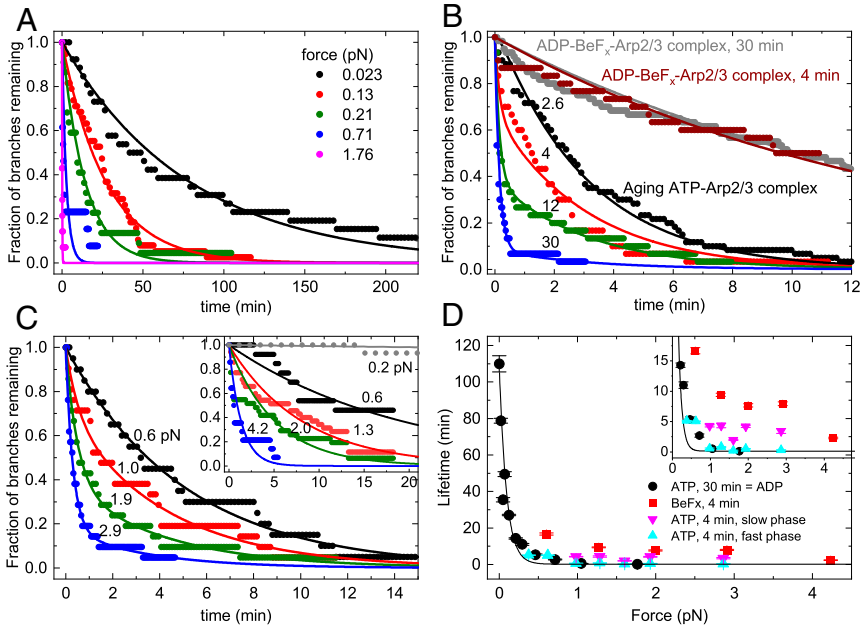

Fig. 2. Effects of mechanical force and nucleotide bound to Arp2/3 complex on the time course of dissociation of actin filament branches. Arp2/3 complex branches were assembled in the flow chamber before applying flow as described in *Materials and Methods*. In *A* and *C*, the force on each observed branch was calculated from its length and the flow rate, and then binned at the indicated average forces values (see *Materials and Methods*). (*A*) The effect of force on the time course of dissociation of actin filament branches formed by ATP-actin monomers and ATP–Arp2/3 complex and aged for 30 min, when most branches had ADP bound to Arp2/3 complex. The fraction of branches remaining is plotted. Smooth curves are the best fits of single exponentials to the data. Each trace includes at least 14 branches. (*B*) Dependence of the time course of dissociation of branches formed with ATP-actin monomers and ATP–Arp2/3 complex with different aging times (2.6, 4, 12, and 30 min) and the presence of BeF_x. For all time courses, 500 μL·min^{-1} of buffer flow was applied to the branches for debranching, producing a force of ∼1 pN for a branch of 1.5 μm. The force on each branch was not calculated for the data shown. Smooth curves are the best global fits of double exponentials to the data for aging branches and yielded two shared rate constants for debranching: slow $k_{s,F} = 0.32$ (±0.005) min^{-1} and fast $k_{f,F} = 6.67$ (±0.44) min^{-1}. Smooth curves are the best single exponential fits to the data for branches aged for 4 and 30 min with BeF_x with lifetimes of 13.9 (±0.2) min^{-1} for the sample aged for ∼4 min and 14.8 (±0.09) min^{-1} for the sample aged for 30 min. Fig. 4*D* presents the fractional amplitudes obtained from the double exponential fits. (*C*) The effect of force on the time course of the dissociation of actin filament branches formed by ATP-actin monomers and ATP–Arp2/3 complex and aged for ∼4 min using the same data collection and analysis methods as in *A*. The smooth curves are best fits of the data to single ($F \leq 0.6$ pN) or double ($F > 0.6$ pN) exponentials. The fractional amplitudes of the slow phase in the time courses that follow the double exponentials are 0.71 ± 0.05 ($F = 0.98$ pN), 0.39 ± 0.06 ($F = 1.29$ pN), 0.81 ± 0.05 ($F = 1.60$ pN), 0.38 ± 0.02 ($F = 1.93$ pN), and 0.17 ± 0.02 ($F = 2.86$ pN). Each trace includes at least 19 branches. (*Inset*) Time courses of branch dissociation under a range of forces for branches formed from ATP–Arp2/3 complex in the presence of 2 mM BeF_x and aged for ∼4 min. Each trace includes at least 13 branches. The smooth curves are single exponential fits to the time courses. Branches dissociate slowly under 0.2 pN of force, so the debranching time course cannot be reliably fitted to obtain the branch lifetime. (*D*) Dependence of branch lifetimes on force for four different conditions: (filled black circles) branches formed from ATP–Arp2/3 complex and aged for 30 min to form branches with ADP–Arp2/3 complex (time courses in *A*); (filled red squares) branches formed from ADP–BeF_x–Arp2/3 complex and aged for ∼4 min (time courses in *C*, *Inset*); (filled pink triangles) slow debranching phase of branches formed from ATP–Arp2/3 complex and aged for ∼4 min (ADP–P_i branch population; time courses in *C*); and (filled blue triangle) fast debranching phase of branches formed from ATP–Arp2/3 complex and aged for ∼4 min (ADP branch population; time courses in *C*). The uncertainty bars for all data represent the SDs from the fits to exponentials shown in *A* and *C*. The smooth black curve is the best single exponential fit (Eq. **1**) to the ADP–Arp2/3 complex debranching data points, yielding a half-force ($F_{1/2}$) of 0.054 (±0.008) pN and branch lifetime in the absence of force (τ_0) of 106 (±8) min (observed rate constant = $\tau_0^{-1} = 0.01$ (±0.007) min^{-1}). *Inset* shows that 1) fast phase lifetimes (blue triangles; 0.3 min to 0.8 min at $F > 1$ pN) differ from the slow phase lifetimes (pink triangles; 2 min to 4 min at $F > 1$ pN; $t = 6.85$, one-tail $t_{critical} = 2.13$ and $P = 0.001$ by Welch's unequal variances *t* test); 2) the slow phase lifetimes (pink triangles; 2 min to 4 min at $F > 1$ pN) differ from the debranching lifetimes with BeF_x (red squares; 8 min to 9 min at $F > 1$ pN; $t = 6.65$, one-tail $t_{critical} = 2.02$ and $P = 0.0006$ by Welch's unequal variances *t* test); and 3) the fast phase lifetimes (blue triangles) do not differ significantly from the debranching with ATP aged for 30 min lifetimes (black circles) at $F > 1$ pN ($t = -0.86$, two-tail $t_{critical} = 2.45$ and $P = 0.42$ by Welch's unequal variances *t* test).

that sustained pN forces reduce τ_{obs} more than two orders of magnitude to <30 s. The force dependence of individual branch lifetimes (*SI Appendix*, Fig. S2) yielded a half-force ($F_{1/2}$) of 0.054 (±0.008) pN and τ_0 = 96 (±6) min, comparable to the values estimated from exponential fits of debranching time courses (Fig. 2 *A* and *D*).

Branches Assembled from ATP–Arp2/3 Complex Dissociate Faster under Force as They Age. As they age, branches assembled from ATP–Arp2/3 complex dissociated progressively faster under force produced by a buffer flow rate of 500 μL·min^{-1} (Fig. 2*B*). Immediately after the 2.6-min assembly reaction, when the dominant nucleotide bound to both Arp2/3 complex and the actin filaments is expected to be ADP–P_i, the time course of branch dissociation followed a single exponential with a slow observed lifetime ($\tau_{s,F}$, where the subscript *F* indicates under flow force) of 3.08 (±0.05) min corresponding to a first-order rate constant $k_{s,F}$ of 0.32 (±0.005) min^{-1}. After aging for 30 min, when both Arp2/3 complex and the subunits in the actin filaments are expected to have bound ADP, the time course of debranching also followed a single exponential with a 20-fold shorter lifetime ($\tau_{f,F}$) of 0.15 (±0.01) min ($k_{f,F}$ = 6.67 (±0.44) min^{-1}). At intermediate aging times, the time courses followed double exponentials (Fig. 2*B*) with distinguishable fast and slow phases, indicating that (at least) two reactions contributed to debranching.

To evaluate how force affects slow and fast debranching, we aged samples for a short time (∼4 min), so the sample would include mixtures of branches with Arp2/3 complex with bound

Table 1. Rate constants for branch formation and dissociation in the absence of force and related figures

Conversion k_{conv} (min^{-1})	State 1 debranching k_1* (min^{-1})	State 2 debranching $k_2^{\dagger}$ (min^{-1})	Branch formation k_{form}* ($\mu M^{-1} \cdot s^{-1}$)
0.14 ± 0.03	0.012	0.01 ± 0.007	0.02
Fig. 4	Fig. 4	Fig. 2*D*	Fig. 4

*The equations used to determine these parameters are approximations, so uncertainties are not reported.

†From the fit of force-dependent debranching data to Eq. **1**; $k_2 = 1/\tau_0$. The error was calculated from the SD τ_0 in the fit.

ADP–P_i and ADP and thus exhibit both slow and fast phases of dissociation over a range of forces applied with different flow rates. However, the actual aging times prior to making observations varied. This uncertainty influenced the observed amplitudes but not the observed lifetimes, so we only analyzed the lifetimes. The debranching time courses at forces of >1 pN followed double exponential decays (Fig. 2*C*), yielding the force dependence of the slow and fast phase lifetimes (Fig. 2 *D* and *Inset*; triangles). The lifetimes of the slow phase (2- to 4-min range) differed from the fast phase (0.3 min to 0.8 min) in this force range (>1 pN), but neither depended strongly on the applied force. At low forces of <0.6 pN, dissociation of branches formed from ATP–Arp2/3 complex followed single exponentials, with lifetimes similar to branches with ADP–Arp2/3 complex (Fig. 2*D*).

The debranching model presented below accounts for these different time courses. The fast phase lifetime behaved similar to ADP–Arp2/3 complex branches (i.e., assembled from ATP–Arp2/3 complex and aged for 30 min), consistent with fast debranching population corresponding to ADP–Arp2/3 complex branches. We discuss the force dependence of the slow phase below.

The Nucleotide Bound to Arp2/3 Complex Influences the Sensitivity of Branches to Force. ATP–Arp2/3 complex hydrolyzes the bound nucleotide upon or soon after branch formation (5, 7) followed by dissociation of the γ-phosphate with an unknown rate constant. Therefore, branches formed by ATP–Arp2/3 complex rapidly transition to the ADP–P_i state for an unknown duration before the release of P_i. Actin filament branches formed by Arp2/3 complex with mutations that slow ATP hydrolysis are more stable than those formed by native Arp2/3 complex, so Martin et al. (10) proposed that the hydrolysis of ATP bound to Arp2/3 complex destabilizes branches.

We performed a series of experiments to determine whether the nucleotide state of Arp2/3 complex could explain the slow and fast debranching states (Fig. 2 *B* and *C*). Like *Acanthamoeba* Arp2/3 complex (5), *Schizosaccharomyces pombe* ADP–Arp2/3 complex did not form branches from ATP-actin monomers nor did the ADP–Arp2/3 complex form branches in the presence of 20 mM phosphate (*SI Appendix*, Fig. S3). A likely interpretation of this behavior is that the transient intermediate ADP–P_i–Arp2/3 complex is competent to form branches, but ADP–Arp2/3 complex binds P_i very weakly (K_d > 20 mM). On the other hand, *S. pombe* ADP–Arp2/3 complex formed branches with 2 mM beryllium fluoride (BeF_x) in the buffer (*SI Appendix*, Fig. S3), as originally shown for *Acanthamoeba* Arp2/3 complex (5). ATP–Arp2/3 complex also forms branches with 2 mM BeF_x in the buffer.

Branches with ADP–BeF_x–Arp2/3 complex dissociate with indistinguishable time courses whether assembled from ATP–Arp2/3 complex or ADP–Arp2/3 complex in the presence of 2 mM BeF_x and aged for ∼4 min (*SI Appendix*, Fig. S4). We assume that, in both cases, BeF_x binds to the ADP–Arp2/3 complex and stabilizes conformations similar to ADP–P_i, as established for actin (27, 28), so we used ADP–BeF_x–Arp2/3 complex branches made with either method. ADP–BeF_x–Arp2/3 complex branches aged for 4 or 30 min in the presence of 2 mM BeF_x dissociate with similar time courses and follow single exponentials (Fig. 2*B*). Thus, branches did not convert from the slowly to the rapidly dissociating state when aged with BeF_x.

Force is required to dissociate, within our experimental observation period, ADP–BeF_x–Arp2/3 complex branches formed from ATP–Arp2/3 complex in the presence of 2 mM BeF_x (Fig. 2 *C*, *Inset*). Under low forces (i.e., <<0.6 pN), <20% of branches with ADP–BeF_x–Arp2/3 complex dissociated within 5 h, so branching lifetimes could not be measured reliably. With forces >0.6 pN, branches dissociated with single exponential time courses and observed rate constants (inverse of lifetimes) that depended on the applied force (Fig. 2 *C*, *Inset*). Therefore, branches with ADP–BeF_x–Arp2/3 complex were more stable under force than branches with ADP–Arp2/3 complex (formed from ATP–Arp2/3 complex and aged for 30 min; Fig. 2*D*).

Under a given force, the lifetimes of ADP–BeF_x–Arp2/3 complex branches were longer (∼twofold) than the slow debranching phase of ATP–Arp2/3 complex branches that had been aged for ∼4 min (Fig. 2*D*). The observed rate constant of the slow phase debranching reflects the sum of the ADP–P_i state debranching rate constant and the rate constant for conversion of the ADP–P_i–Arp2/3 complex to the ADP state (see *Discussion*).

It is therefore expected to be faster than ADP–BeF_x–Arp2/3 complex debranching, which converts more slowly to ADP–Arp2/3 complex (Fig. 2*B*).

The Nucleotide State of the Actin Filaments Does Not Influence Debranching. We assembled branches from ATP–Arp2/3 complex with ADP or ADP–P_i bound to the subunits in the actin filaments and observed that all had similar time courses of debranching after aging for a given time (*SI Appendix*, Fig. S5). Samples with ADP-actin filaments were prepared by assembly from ATP-actin monomers and ATP-actin Arp2/3 complex followed by aging for 30 min. Samples with ADP–P_i actin filaments were prepared by assembly from ATP-actin monomers and ATP–Arp2/3 complex in buffer containing 20 mM phosphate followed by aging for 4 or 30 min (*SI Appendix*, Fig. S5). This concentration of phosphate is well above the K_d for binding ADP-actin subunits (29), so subunits in the filaments likely had ADP–P_i in the active site, assuming that Arp2/3 complex binding does not dramatically change the affinity of actin for phosphate. Samples assembled from ATP-actin monomers and ATP–Arp2/3 complex followed by ∼4 min of aging had a mixture of ADP and ADP–P_i nucleotide states for both actin subunits and Arp2/3 complex. Samples with AMPPNP actin (a nonhydrolyzable analog of ATP) were assembled from AMPPNP actin monomers and ATP-actin Arp2/3 complex in buffer containing 2 mM AMPPNP followed by aging for ∼4 min. Since AMPPNP–Arp2/3 complex does not form branches (ref. 5 and *SI Appendix*, Fig. S3), all of the branches formed from Arp2/3 complex with bound ATP, while the actin filaments had bound AMPPNP. A previous study of bovine Arp2/3 complex (16) reported more branches on mother filament segments with ADP–P_i than segments with ADP. This difference was attributed to slower dissociation of branches aged in buffer with 25 mM phosphate allowing time for them to be stabilized by binding to the slide coated with *N*-ethylmaleimide (NEM)-myosin anchors. However, that study did not measure time course of the dissociation of branches, and we did not compare the rate of branch formation on ADP and ADP–P_i mother filaments, so we do not know whether the sources of Arp2/3 complex, the presence of NEM-myosin anchors on the surface, or other factors account for the apparent difference.

Since the debranching kinetics are independent of the nucleotide (i.e., ADP, ADP–P_i, or AMPPPNP) bound to the mother and daughter filaments, the stabilization of branches by BeF_x (Fig. 2 *B–D*) is likely due to BeF_x bound to Arp2/3 complex in the branch junction. This suggests that the ADP–P_i–Arp2/3 complex intermediate has different mechanical properties than the ADP–Arp2/3 complex after phosphate dissociation. The lack of an effect of 20 mM phosphate on debranching (*SI Appendix*, Fig. S5) is consistent with the affinity of *S. pombe* ADP–Arp2/3 complexes in branch junctions for phosphate being very weak (K_d > 20 mM).

Force Promotes but BeF_x Inhibits Debranching by GMF. GMF (20–22) promotes the dissociation of actin filament branches without applied force, so we measured how the concentration of fission yeast GMF influences the rates of dissociation of actin filament branches with ADP–BeF_x–Arp2/3 complex or ADP–Arp2/3 complex at a low buffer flow rate (15 μL·min^{-1}). This flow rate exerts very little force on branches and had little or no effect on debranching (Fig. 2).

Concentrations of GMF up to 1 μM did not dissociate branches with ADP–BeF_x–Arp2/3 complex (Fig. 3*A*), but nanomolar concentrations of GMF promoted dissociation of branches with ADP–Arp2/3 complex (Fig. 3). Time courses of dissociation of branches with ADP–Arp2/3 complex followed single exponentials (Fig. 3*A*) with lifetimes (τ_{obs}) that depended hyperbolically on the concentration of GMF (Fig. 3*B*).

Force increased the rate at which GMF dissociated branches with ADP–Arp2/3 complex (*SI Appendix*, Fig. S6), but dissociation was slower than predicted if GMF and force increased the rate of dissociation independently (i.e., their energetic contributions to debranching were additive). This raises the possibility that the reactions catalyzed by force and GMF are coupled and/or that debranching follows different pathways in the presence absence of force.

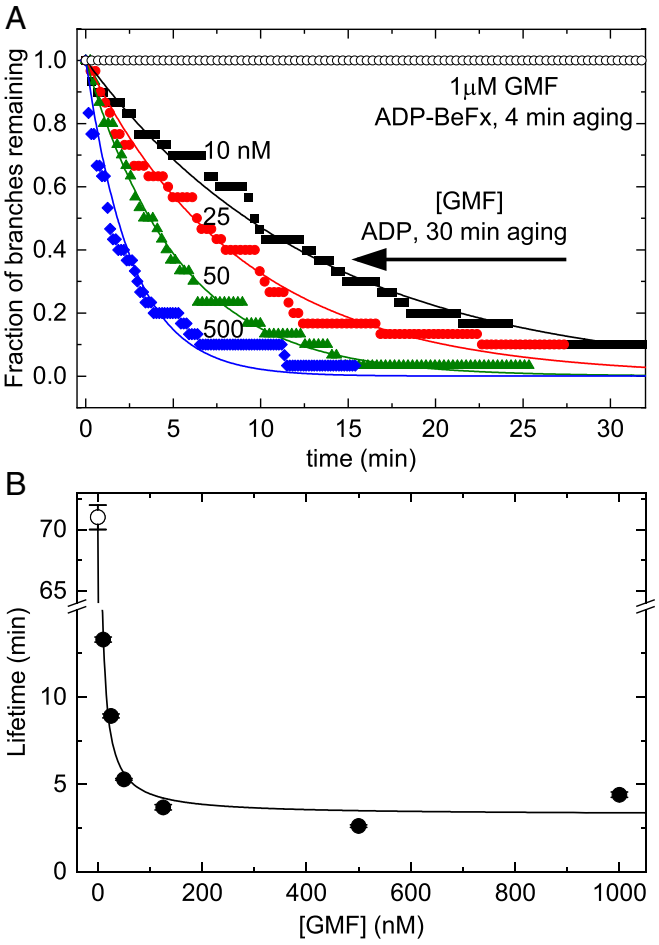

Fig. 3. BeF_x inhibits debranching by GMF. (*A*) Dependence of the time course of dissociation of branches with ADP–BeF_x–Arp2/3 complex or ADP–Arp2/3 complex on the concentration of GMF. Branches with ADP–BeF_x–Arp2/3 complex were assembled in buffer containing 0.2 mM ATP, 2 mM $BeSO_4$, and 10 mM NaF and aged for ∼4 min. Branches with ADP–Arp2/3 complex were assembled in buffer with 0.2 mM ATP and aged for 30 min to allow for ATP hydrolysis and phosphate dissociation (Fig. 2*B*). Debranching was initiated by flowing buffer with GMF at 15 μL·min^{-1} and continued throughout the debranching measurements. The smooth curves are the best fits of single exponentials to the data, yielding the (average) branch lifetimes; n = 30 branches for each trace. A concentration of 1 μM GMF did not dissociate branches with ADP–BeF_x–Arp2/3 complex assembled from ATP-actin and ATP–Arp2/3 complex with BeF_x and aged for ∼4 min (open black circles). (*B*) Dependence of the lifetimes of branches with ADP–Arp2/3 complex on the concentration of GMF at a buffer flow rate of 15 μL·min^{-1}. The line is the best fit of Eq. **3** to the data, yielding a GMF binding affinity ($K_{d,GMF}$) of 40 (±10) nM and a maximum debranching rate constant ($k_{diss,GMF}$) of 0.31 (±0.05) min^{-1}. At this low flow rate, branches with ADP–Arp2/3 complex (without GMF) dissociated with a rate constant ($k_{diss,0}$ = 0.014 ± 0.0002 min^{-1}, indicated by an open circle) similar to that under zero force (Fig. 2*B* and Table 1). The uncertainty bars are within the data points and represent the SDs of lifetimes in the best single exponential fits of time traces in *A*.

Discussion

Quantitative Analysis of the Two-State Model for Dissociation of Actin Filament Branches. Our experiments show that the nucleotide bound to Arp2/3 complex determines the sensitivity of branches to dissociation by physical force. We use a formal description of a simple two-state model (Fig. 4*A*) to analyze our data and estimate the rate constants for the three reactions and their sensitivities to force.

Description of the model. The model (Fig. 4*A*) assumes that branches form when ATP–Arp2/3 complex binds to the side of a mother filament and nucleates a daughter filament growing at its barbed end. Hydrolysis of ATP in the active sites of *Acanthamoeba* Arp2/3 complex is closely associated with nucleation of the daughter filament (5, 7), so we assume that state 1 branches have Arp2/3 complex with bound ADP–P_i. Dissociation of the γ-phosphate with a rate constant k_{conv} converts branch state 1 to branch state 2 with ADP bound to Arp2/3 complex. Branches in either state can dissociate from the mother filament. The model predicts that, overall, net debranching time courses follow double exponentials with two rate constants. One observed rate constant is the sum of the rate constants for state 1 debranching and conversion ($k_{\mathrm{obs},1(F)} = k_{1(F)} + k_{conv(F)}$; ($F$) indicates optional force). The second observed rate constant corresponds to debranching of state 2 ($k_{\mathrm{obs},2(F)} = k_{2(F)}$; *SI Appendix*, Eqs. **S25** and **S29**). Force accelerates the dissociation of branches with either ADP–Arp2/3 and ADP–P_i–Arp2/3 complex, but branches with ADP–P_i or ADP–BeF_x–Arp2/3 (mimicking the ADP–P_i state) complex are much more resistant to force than branches with ADP–Arp2/3 complex. As branches age, phosphate release converts slowly dissociating, "young and strong" state 1 branches with ADP–P_i–Arp2/3 complex into rapidly dissociating, "old and weak" state 2 branches with ADP–Arp2/3 complex.

Formulation of the model. We analyzed the experimental data using a parallel debranching pathway (Fig. 4*A* and *SI Appendix*, *Part 2* and Scheme S1) where "young" (strong, state 1) branches convert to "old" (weak, state 2) branches as they age (Fig. 4*A*). We fit the aging time dependence of the fractions of slowly and rapidly dissociating branches observed under force as the amplitudes ($A_{s,F}$ and $A_{f,F}$, respectively; Fig. 4*C*) of double

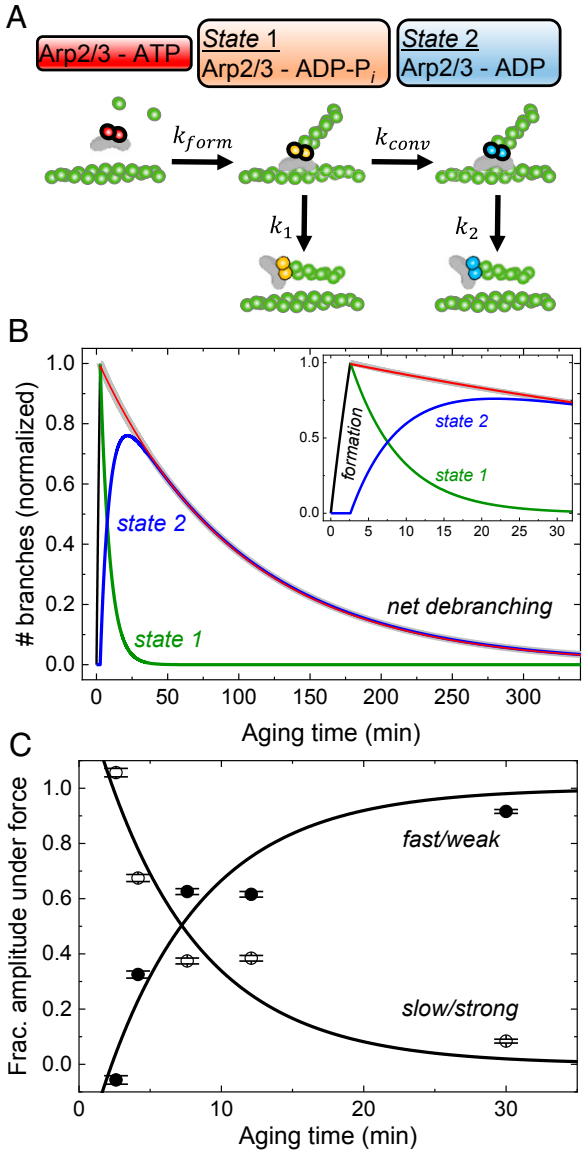

Fig. 4. Model and simulations of the pathways of branch formation, aging, and debranching. (*A*) Schematic of our hypothesis. Formation of a branch by ATP–Arp2/3 complex (red) is coupled to hydrolysis of ATP bound to the Arps (5, 7) with rate constant k_{form}, yielding ADP–P$_i$–Arp2/3 complex (orange) in state 1. Irreversible phosphate dissociation with rate constant k_{conv} converts state 1 to ADP–Arp2/3 complex (blue) in state 2. Branches dissociate from mother filaments with rate constants k_1 for state 1 and k_2 for state 2, both sensitive to force. (*B*) Simulated time course of the model showing how the populations of state 1 branches, state 2 branches, and dissociated branches evolve over time in the absence of force. We assumed that Mg-ATP-actin monomers and Mg-ATP–Arp2/3 complex formed branches for 2.6 min, when the free proteins were removed, and the reactions continued without additional branch formation. The red line represents the best single exponential fit to the observed debranching (i.e., combined from both states) starting with a normalized value of 1 at the end of branch formation (2.6 min). The experimentally determined or estimated rate constants used in the simulation are $k_{form}[Arp] = 0.12$ min^{-1}, $k_{conv} = 0.14$ min^{-1}, $k_1 = 0.012$ min^{-1}, and $k_2 = 0.01$ min^{-1}. (*C*) Aging time dependence of the fractional the slow and fast phase amplitudes in the debranching time courses under 500 μL·min^{-1} of buffer flow, obtained from double exponential fits to the time courses (Fig. 2*B*). These data were used for extraction of fundamental rate constants in Table 1. The best global fits of the two-state model (Eq. **2**) to the fractional amplitude data gave rate constants for conversion k_{conv} of 0.14 min^{-1}, state 1 branch dissociation k_1 of 0.012 s^{-1}, and branch formation k_{form} of 0.02 μM^{-1}·s^{-1} without force (Table 1). The one negative fast phase amplitude at 2.6 min results from a net increase in the state 2 branch population during debranching under force after 2.6 min aging time. The state 2 branch population is the net sum of depletion from debranching (negative contribution to population, exponential decay) and gain from conversion of state 1 branches (positive contribution, exponential rise). For short aging times, little or no state 2 branches exist for depletion, and the conversion from state 1 branches, represented by an exponential rise (negative amplitude), dominates the time course (54, 55). The uncertainty bars are SDs of the fractions of branches from the global double exponential fits of debranching time courses with different aging times in Fig. 2*B*.

exponential fits to the following functions (*SI Appendix*, Eqs. **S34** and **S37**):

$$A_{s,F} = \frac{be^{-(k_{conv}+k_1-k_2)(t_{age}-t_1)}}{1+ae^{-(k_1+k_{conv}-k_2)(t_{age}-t_1)}}$$
$$A_{f,F} = \frac{1+(a-b)e^{-(k_{conv}+k_1-k_2)(t_{age}-t_1)}}{1+ae^{-(k_1+k_{conv}-k_2)(t_{age}-t_1)}} = 1-A_{s,F} \quad [2]$$

where t_1 is the 2.6 min during which branches formed from ATP–Arp2/3 complex and ATP-actin monomers, t_{age} is aging time, the intrinsic debranching rate constants are k_1 for state 1 and k_2 for state 2 in the absence of force, and k_{conv} is the rate constant for conversion of state 1 to state 2 in the absence of force (Fig. 4*A* and *SI Appendix*, *Part 2* and Scheme S1). The constants a and b are unitless composites of rate constants and initial branch concentrations defined in *SI Appendix*, *Part 2* and Scheme S1 (*SI Appendix*, Eqs. **S39** and **S40**). The constant a is force independent and determined only by intrinsic debranching in the absence of an applied force (*SI Appendix*, Eq. **S39**). The constant b is a function of debranching and conversion under force (*SI Appendix*, Eq. **S40**), yielding force-dependent amplitudes ($A_{s,F}$ and $A_{f,F}$) when debranching and/or conversion are force dependent.

Estimation of the rate constants for branch formation and phosphate dissociation. Global analysis of the data (Figs. 2*B* and 4*C* and *SI Appendix*, *Part 2*) yielded an overall pseudo–first-order association rate constant for branch formation of 0.12 min^{-1} (*SI Appendix*, *Part 2*). Given 100 nM Arp2/3 complex used in our experiments, we estimate the second-order association rate constant for Arp2/3 complex binding to mother filaments and subsequent activation (k_{form}) to be ~0.02 μM^{-1}·s^{-1} (Table 1), consistent with published reports (30–32).

The best fit of the fractional amplitudes to Eq. **2** (Fig. 4*C*) yielded a rate constant (k_{conv}) of 0.14 (±0.03) min^{-1} (corresponding to a lifetime of >7 min) for conversion of state 1 branches to state 2 branches. We interpret the conversion reaction as the release of P$_i$ from the Arp2/3 complex, and thus interpret state 2 branches as ADP–Arp2/3 complex branches. This rate constant inferred for P$_i$ release from ADP-P$_i$ Arp2/3 complex is similar to the rate constant of ~0.18 min^{-1} for P$_i$ release from actin filaments (29).

We can place a limit on the rate constant for phosphate binding to ADP-Arp2/3 complex in a branch junction (k_{+Pi}). We interpret conversion to reflect P$_i$ release, so $k_{-Pi} = k_{conv} = 0.14$ (±0.03) min^{-1}, and know that P$_i$ binds Arp2/3 complex in branches with a low affinity ($K_d > 20$ mM; *SI Appendix*, Fig. S5*A*). Therefore, the second order association rate constant of k_{+Pi} is less than 7 M^{-1} min^{-1} = 0.12 M^{-1} s^{-1}. This value is two orders of magnitude slower than P$_i$ binding to ADP-actin subunits in the interior of filaments [600 M^{-1}min^{-1} = 10 M^{-1}s^{-1} (29)].

Estimation of the rate constants for branch dissociation at low force. The rate constant for dissociation of state 2 branches at zero force is $k_2 \approx 0.01$ min^{-1}, based on the intercept of the force-dependence of ADP-Arp2/3 complex (state 2) branch lifetimes (Fig. 2*D*). The rate constant for debranching from state 1 at zero force (k_1) is ~0.012 min^{-1}, from the analysis of the aging time-dependence of

time course of dissociation of branches (Figs. 2*B* and 4*C*, Table 1, and *SI Appendix*, *Part 2* and Eq. **S42**). As a result of these two rate constants being similar ($k_1 \approx k_2$), debranching without force follows a single exponential with a rate constant of ~k_2 (*SI Appendix*, *Part 2* and Eq. **S25** and Fig. 4*B*), even though three reactions (conversion and debranching from state 1 and state 2) occur simultaneously.

Time courses also follow single exponentials at low forces (<0.6 pN), independent of the aging time (Fig. 2 *C*and *D*). This behavior arises because dissociation is much slower than conversion ($k_1 << k_{conv}$), so ADP-P_i branches convert to ADP before dissociating. At forces >1 pN, the observed dissociation time courses follow double exponentials because $k_{conv} < k_1$ and debranching occurs from both ADP-P_i and ADP branches.

Estimation of the force sensitivity of the branch dissociation rate constants. Force increases the dissociation rate constants of both branch states, but has a larger effect on state 2 branches with ADP-Arp2/3 complexes than state 1 branches with ADP-P_i-Arp2/3 complexes (Fig. 2*D*). The best global fits of the double exponential time courses at intermediate aging times yielded a ~20-fold difference in the lifetimes of the species that dissociated slowly ($k_{s,F} = 0.32$ (±0.005) min^{-1}) and rapidly ($k_{f,F} = 6.67$ (±0.44) min^{-1}) at a buffer flow rate of 500 μL min^{-1} (Fig. 2*B*). Under this force, the observed fast rate constant is the rate constant for the state 2 branch dissociation (i.e., $k_{f,F} = k_{2,F}$) and the observed slow rate constant is the sum of the rate constants for dissociation for state 1 branches and conversion from state 1 to state 2 (i.e., $k_{s,F} = k_{1,F} + k_{conv,F}$; *SI Appendix*, *Part 2* and Eqs. **S29** and **S41**).

Force produced by a flow of 500 μL min^{-1} increased the observed dissociation of branches ~670-fold (from $k_2 = 0.01$ to $k_{2,F} = 6.67$ min^{-1}) for those with ADP-Arp2/3 complex but only 32-fold (from $k_1 = 0.012$ to $k_{1,F} = k_{s,F} - k_{conv,F} < k_{s,F} = 0.32$ min^{-1}; Fig. 2*B* and *SI Appendix*, Fig. S5) for those with ADP-P_i-Arp2/3 complex. This difference in force sensitivity of the two states explains the dramatic acceleration in overall debranching with aging (Fig. 2*B*). Furthermore, we estimate that force produced by 500 μL min^{-1} flow increased k_{conv} only two-fold from $k_{conv} = 0.14$ min^{-1} in the absence of force to $k_{conv,F} = k_{s,F} - k_{1,F} < k_{s,F} = 0.32$ min^{-1} in the presence of force (*SI Appendix*, Fig. S5).

Implications of the Force Sensitivity of Branches for Their Turnover in Cells.

Implications for debranching by myosin motor proteins. A sustained flow force of ~1 pN dissociates ADP-Arp2/3 complex branches in <30 s (Fig. 2*D*), raising the possibility that pN contractile forces generated by myosin motors could rapidly debranch and reorganize Arp2/3 complex networks. Myosin accelerates network disassembly and reorganization in both biomimetic systems (33, 34) and in cells (35, 36). We note, however, that the work (i.e., energy term) from the applied force determines the overall debranching acceleration, not the force per se.

Implications of Nucleotide-Dependent Force Sensitivity of Arp2/3 Complex Debranching. "Young" branches with ADP–P_i–Arp2/3 complex are more resistant to dissociation by force than "old" branches with ADP–Arp2/3 complex. Nucleation-promoting factors associated with membranes (plasma membrane, vesicles, intracellular bacteria) activate Arp 2/3 complex, so "young" branches are located closer to these surfaces than "old" branches. If force is uniformly distributed across the filament network, old branches farthest from the surface with nucleation-promoting factors would be preferentially debranched.

This differential response to force may contribute to the observed remodeling of cellular branched actin networks under load, including local changes in branch density (13–15). We apply a simple a minimal kinetic model (*SI Appendix*, *Part 3*) to analyze how selective, force-sensitive debranching might influence the distribution of branches in actin networks at the leading edge of cells. The model assumes Arp 2/3 complex is activated uniformly at the membrane, such that the branch density distribution is also uniform, on average, along the plane parallel to the cell membrane at the leading edge. The model with the experimental parameters determined here predicts that the density of branches decays exponentially (see also refs. 37–39) along the axis perpendicular to the membrane, toward cell interior in both the absence and presence of force, but preferential debranching of old Arp 2/3 complexes shortens the branch density decay length and can, under some conditions, increase the local branch density near the membrane (*SI Appendix*, *Part 3* and Figs. S9 and S10). Thus, external force on the leading edge of cells favors debranching of old branches that have migrated toward the cell interior over young branches still near the membrane and can thus contribute to spatial and vectorial network turnover. External force may also influence binding of cofilin (40) and GMF (Fig. 3; discussed below), both of which display debranching activity (20, 24).

GMF Selectively Dissociates ADP–Arp2/3 Complex Branches. Fission yeast GMF increases the rate constant for dissociation of branches with ADP–Arp 2/3 complex up to ~20-fold, but does not dissociate branches with ADP–BeF_x–Arp 2/3 complex (Fig. 3). The following parallel reactions describe GMF-catalyzed dissociation of branches with ADP–Arp2/3 complex:

$$\begin{array}{ll} Arp + GMF \rightleftharpoons Arp\text{-}GMF & \downarrow k_{diss,0} \\ \downarrow k_{diss,GMF}, & \text{debranched} \end{array}$$

Scheme 1

where $k_{diss,0}$ and $k_{diss,GMF}$ are the dissociation rate constants of branches formed by Arp2/3 complex alone (*Arp*) and GMF-bound Arp2/3 complex (*Arp-GMF*), and $K_{d,GMF}$ is the affinity of GMF for Arp 2/3 complex in a branch junction. This scheme assumes that GMF binding equilibrates rapidly compared to the rate of debranching (and $k_{+GMF}[GMF]$, $k_{-GMF} >> k_{diss,0}$, $k_{diss,GMF}$) and that $[GMF] >> [Arp2/3\ complex]$.

Debranching from the parallel pathway in Scheme 1 follows a single exponential (41). The dependence of the observed branch lifetime (τ_{obs}) on the concentration of GMF can be expressed in two ways, first,

$$\tau_{obs} = \tau_0 - \frac{(\tau_0 - \tau_{GMF})[GMF]}{K_{d,GMF}\left(\frac{\tau_{GMF}}{\tau_0}\right) + [GMF]}. \quad [3]$$

Alternatively, the relationships can also be expressed in terms of observed rate constants (41, 42),

$$k_{obs} = k_0 + \frac{(k_{GMF} - k_0)[GMF]}{K_{d,GMF} + [GMF]}. \quad [4]$$

The best fit of Eq. **3** to the dependence of the observed branch lifetime (τ_{obs}) on the concentration of GMF (Fig. 3*B*) yielded an apparent affinity of GMF for ADP–Arp2/3 complex ($K_{d,\ GMF}$) of 40 (±10) nM and a lifetime of GMF bound to ADP–Arp2/3 complex in branches (τ_{GMF}) of 3.3 (±0.5) min. This corresponds to a debranching rate constant ($k_{GMF} = 1/\tau_{GMF}$) of 0.31 (±0.05) min^{-1}. In Eqs. **3** and **4**, k_0 is the debranching rate constant and τ_0 is the branch lifetime without GMF under very low flow rate (15 μL·min^{-1}), that is, very low average force. The best fit yielded $k_0 = 1/\tau_0 = 0.014$ (±0.0002) min^{-1}, corresponding to $\tau_0 = 71$ (±1) min. These values are slightly faster than the intrinsic dissociation rate constant for branches with ADP–Arp2/3 complex in the absence of force (>100 min; Fig. 3) due to the 15 μL·min^{-1} flow rate employed in this experiment. We note, for general readers, that the GMF concentration at half-maximum

effect is given by $K_{d,GMF}$ (τ_{GMF}/τ_0) in Eq. **3** and $K_{d,GMF}$ in Eq. **4**, so its value differs depending on how the data are plotted.

Reported affinities of GMF for soluble Arp2/3 complex ($K_{d,GMF}$) vary widely: >>10 μM for ATP–Arp 2/3 complex (43); 0.7 μM for ADP–Arp2/3 complex (43); and 13 nM (20–22) or ∼1 μM (44) for Arp2/3 complex without a specified nucleotide. We found that the measured affinity of GMF for Arp2/3 complex in branch junctions bound to both a mother and daughter filament depended on the bound nucleotide. Arp2/3 complex used in these studies came from different organisms: *Saccharomyces cerevisiae* (20–22), bovine brain (43), and *S. pombe* (this study and ref. 44).

Thus, GMF preferentially dissociates "old" branches with ADP–Arp2/3 complex rather than "young" branches with ADP–P_i–Arp2/3 complex. Given that GMF has a much lower affinity for ATP–Arp2/3 complex in solution than ADP–Arp2/3 complex (43), weak binding of GMF to ADP–P_i–Arp2/3 complex in branches is the most likely explanation for the resistance of young branches and branches with ADP–BeF_x–Arp2/3 complex to dissociation by GMF. The nucleotide bound to Arp2/3 complex might also affect the debranching reaction directly.

Saturating GMF destabilizes ADP–Arp2/3 complexes, reducing their lifetime from more than 60 min to ∼3 min (Fig. 3). While GMF strongly promotes debranching, these long lifetimes (3 min) at saturating GMF concentrations place limits on the role of GMF in mediating debranching and network turnover in cells. More-rapid debranching may be achieved by combining GMF with force and/or from contributions from other debranching proteins such as cofilin, which dissociates branches on a second time scale at micromolar concentrations without force (24).

Arp2/3 Complex Likely Dissociates with the Daughter Filament. A daughter filament and its associated Arp2/3 complex dissociate simultaneously (within the 100 ms time resolution of our experiments) during debranching events. We cannot eliminate a pathway in which the daughter filament detaches first, followed by rapid release of Arp2/3 complex. However, we favor a mechanism where the interface between Arp2/3 complex and the mother filament ruptures and simultaneously releases the daughter filament with Arp2/3 complex on its pointed end. This mechanism is consistent with actin filaments rarely fragmenting under debranching conditions, so the rate constant for rupture of the actin–actin interface is hundreds of times slower than the rate constant for rupturing a branch junction. Given that the interface between Arp2/3 complex and the daughter filament is structurally similar on many levels to an actin–actin interface (45), it is likely to rupture slowly like actin filaments.

Materials and Methods

Protein Purification. Rabbit skeletal muscle actin was purified from back and leg muscles and labeled on lysine residues with NHS esters of Alexa 568, Alexa 647, or biotin (46, 47) or on Cys-374 with pyrene iodoacetamide (48). Actin monomers with bound ATP were passed twice through a desalting column to exchange into G-Buffer (20 mM Tris pH 8, 2 mM $CaCl_2$, 10 mM NaN_3, 0.2 mM ATP, and 0.5 mM dithiothreitol [DTT]) containing 0.2 mM AMPPNP instead of ATP and incubated for 1 h at 25 °C. Remaining free nucleotides were removed with a desalting column in G-Buffer containing AMPPNP instead of ATP prior to polymerization experiments. Arp2/3 complex was stored in ATP buffer solution composed of 10 mM Pipes at pH 6.8, 100 mM KCl, 1 mM $MgCl_2$, 0.25 mM ethylene glycol bis(β-aminoethyl ether)-*N*,*N*,*N*′,*N*′-tetraacetic acid [EGTA], 0.1 mM ATP, and 1 mM DTT.

Recombinant fission yeast glutathione *S*-transferase (GST)-VCA was purified from bacteria (49). *S. pombe* Arp2/3 complex was purified from the TP150 strain, a protease-deleted *S. pombe* strain (49). Fluorescent Arp2/3 complex was generated by conjugating Alexa 488 to a snap tag on the C terminus of the Arpc5 subunit. Bulk polymerization assays with pyrenyl actin and GST-VCA showed that Arp2/3 complex with 82% labeling of the snap tag nucleated 91% as many actin filaments as unlabeled Arp2/3 complex (4.2 nM vs. 4.6 nM of barbed ends at half-maximal polymerization; *SI Appendix*, Fig. S6) (refs. 48 and 49 and *SI Appendix*, Fig. S8).

A complementary DNA for *S. pombe* GMF was cloned and inserted into the pet28a plasmid that includes GST and Tobacco Etch Virus (TEV) protease sites. Recombinant GMF was expressed in Rosetta2 BL21 *Escherichia coli* cells (Novagen) and purified using glutathione affinity chromatography. After cleaving off GST with TEV protease, a second round of glutathione chromatography removed the protease and GST. After fast protein liquid chromatography on a MonoQ column (20), the GMF was greater than 95% pure when analyzed by sodium dodecyl sulfate polyacrylamide gel electrophoresis.

Microscopy and Microfluidics. A total internal reflection fluorescence (TIRF) microscopy system with a Till iMic digital microscope equipped with a ×100 objective (Olympus) and an Andor iXon897 electron multiplying charge-coupled device (EMCCD) camera was used in this study. Images were acquired at a rate of 5 to 30 frames per second. Coverslips were cleaned with the following solutions, all incubated in a sonicator for 30 min and rinsed intensively with Milli-Q water in between steps: 2% Hellmanex, water, acetone, 1 M HCl, 5 M KOH, and hexane, then silanized with 650 μL of dichlorodimethyl silane in 500 mL of hexane for 30 min, and subsequently rinsed and sonicated in hexane for 3 × 1 min. Coverslips were dried using a stream of nitrogen gas and stored in falcon tubes at −20 °C for up to 2 mo (50).

A glass microfluidic chamber was constructed as described in ref. 51. Briefly, the input and output ports for flow solution were formed in polydimethylsiloxane (PDMS) using a flat-tip needle. Holes connecting the PDMS to parallel sample chambers were drilled through the glass with a diamond tip bit. Subsequently, a plasma cleaner was employed to bond PDMS to slide glass. Immediately before use, chambers were assembled using parafilm on the glass slide opposite to PDMS ports, and a coverslip was placed over the parafilm and sealed with heat.

A fixed rate hydrodynamic flow exerted by an automatic syringe pump applied pulling forces on actin filaments. The magnitude of pulling force on a branch joint ($\mathbf{F_d}$; *SI Appendix*, Fig. S1 *A* and *B*) scales with daughter filament branch length and flow rate. These values span a range up to a few piconewtons for the daughter filament lengths and flow rates examined here. Pulling force was calculated according to the Batchelor (52) equation,

$$F_d = \eta \frac{2\pi l v}{\ln\left(\frac{2h}{r}\right)}. \quad [5]$$

Eq. **5** estimates drag force on a cylindrical filament with correction for the height (h) of the filaments from the surface of the flow chamber (53). Solution viscosity (η) is assumed to equal unity; l is the (daughter) filament length and varies for individual branches. The average actin filament radius is $r = 4$ nm, and v is the linear fluid velocity in the plane of the filament. We assume an average height (h) of 200 nm from the flow chamber surface. The fluid velocity (v) is proportional to bulk flow rate and was determined from the movement of 100 nM TetraSpek beads (Thermo Fisher) through the sample chamber (52). Only beads moving parallel to the surface were employed in our analysis, as the flow velocity profile changes with the height from the chamber surface. Bead flow velocity was measured via ImageJ "Manual Tracking" and used in force calculations (52). In the experiments presented in Fig. 2 *A* and *C*, multiple experiments at different flow rates were performed, and the force on each branch was calculated using the flow rate and length of the branch. Then, debranching data from different flow cells with a range of flow rates were binned according to the force on each branch and plotted as survival time courses, given by the fraction of branches remaining at each time point. For example, the branches in Fig. 2*A* were divided into bins of at least 13 branches. The bin size for each data point is approximately the midpoint between the point itself and its neighboring data points (Fig. 2*D*). At low forces (0.002 pN to 0.4 pN), the bin sizes were small, for example, 0 pN to 0.04 pN, 0.1 pN to 0.2 pN, etc., and, at higher forces (>∼1 pN), the bin sizes were larger, for example, 0.8 pN to 1.4 pN, 1.4 pN to 2.4 pN, etc.

Some of these parameters are uncertain, so the estimated force values may be offset systematically for all of our experiments. The least certain parameter is the distance of individual filaments from the surface, which may vary by <50% from the average distance of 200 nm assumed here. A 500 μL·min^{-1} flow rate produces forces on a 1.5-μm branch of 0.94 pN at a height of 300 nm, 1.02 pN at 200 nm, and 1.20 pN at 100 nm (SI appendix in ref. 52). Therefore, the absolute forces and parameters calculated from them may be imprecise, but no more than 20%, and the relative forces between experiments can be compared.

Preparation of Branched Actin Filament Networks and Experimental Procedures. KMIE buffer (6, 23) (10 mM imidazole pH 7.0, 50 mM KCl, 2 mM $MgCl_2$, 1 mM EGTA, 0.2 mM ATP, 2 mM DTT) supplemented with

15 mM glucose, 0.02 mg·mL^{-1} catalase, and 0.1 mg·mL^{-1} glucose oxidase was used for all microscope experiments, unless noted otherwise. Filaments of Alexa 568–labeled actin (Fig. 1*A*, red filament segment; 15% labeled with Alexa 568 and containing 10% biotinylated actin subunits) were polymerized in KMIE buffer, sheared by vigorous pipetting, and subsequently mixed with 1.5 μM Alexa 647-labeled actin monomers (Fig. 1*A*, green segment and branch), 0.1 μM Arp2/3 complex, and 0.5 μM GST-VCA in KMIE buffer. This solution was incubated for 1 min to 2 min to initiate branch formation. During the branching reaction, green actin monomers elongated from either the barbed end of short Alexa 568 actin segments or mother filament bound Arp2/3 complex VCA, forming mother or daughter filaments, respectively. This mixture was pipetted into flow chambers where the short, red actin segments bind the neutravidin-coated coverslip surface, and the branching reaction was allowed to continue for 1 min to 2 min. The total time of branch formation and aging for a given experiment (e.g., 2.6 min) is indicated in the text. Branch formation and filament elongation was then terminated by removing untethered proteins (labeled actin, Arp2/3 complex, and GST-VCA) from the sample chamber with gentle flow of KMIE buffer. Tethered filaments were further aged for different time periods after the removal of unbound protein. Low (2 μL·min^{-1}) flow applied during aging ensured irreversible debranching. Filament segments with Alexa 568 actin subunits (Fig. 1*A*, red) were tethered to the surface, while Alexa 647 actin (Fig. 1*A*, green) mother and daughter filaments were allowed to freely fluctuate and align with flow. Unlabeled actin monomer (0.2 μM) was included in flow buffer solution to prevent filament depolymerization. The "aging time" specified in each experiment is the time between the initial mixing of the proteins and application of debranching flow, including the time for branch formation and further aging. The age times were precisely measured in the experiment in Fig. 2*B* but are approximate times in all other experiments. Debranching under force was performed by applying flow at a fixed rate (specified in text) throughout the experiment. Since unbound proteins were removed after the branch formation period, actin filament elongation was terminated, and individual branch length (l) and consequently applied force (F) on the branch joint were constant (Eq. **5**).

Experiments with BeF_x were performed two different ways. 1) For experiments with ATP–Arp2/3 complex (Fig. 2 *C*, *Inset*), branches were formed from ATP-actin monomers and ATP–Arp2/3 complex as described above but with 2 mM $BeSO_4$ and 10 mM NaF included in the buffer at all times, and aged for ∼4 min before applying various rates of flow with KMIE buffer supplemented with 2 mM $BeSO_4$ and 10 mM NaF. For the experiment with BeF_x and 30-min aging (Fig. 2*B*, gray), ATP–Arp2/3 complex branches were formed as described above and aged for 30 min with 2 mM $BeSO_4$ and 10 mM NaF before applying flow with KMIE buffer. 2) For experiments with ADP–Arp2/3 complex and BeF_x (Fig. 2*B*, brown), mother filaments with ATP-actin (10% biotinylated) monomers were immobilized on the surface as described above, and the KMIE buffer (which includes ATP) was washed out and replaced with KMIE ADP buffer supplemented with 2 mM $BeSO_4$ and 10 mM NaF. Then ADP-actin monomers, ADP–Arp2/3 complex, and GST-VCA in KMIE buffer with 2 mM $BeSO_4$ and 10 mM NaF and 2 mM ADP instead of 2 mM ATP were gently flowed into the chamber and allowed to form branches. After a ∼4-min branch formation period, all unbound proteins were washed out with KMIE ADP and 2 mM $BeSO_4$ and 10 mM NaF and maintained under flow as noted. ADP-actin and ADP–Arp2/3 complex were prepared by exchanging nucleotide from ATP-actin and ATP–Arp2/3 complex, respectively, using desalting columns. ADP–Arp2/3 complex never formed branches unless 2 mM $BeSO_4$ and 10 mM NaF was present as reported previously and shown here (*SI Appendix*, Fig. S3) (5, 6).

For experiments with AMPPNP mother filaments, filaments were polymerized from AMPPNP actin monomers and immobilized on the surface as described above. Branch formation was initiated with ATP–Arp2/3 complex as described above in KMIE buffer with 0.2 mM AMPNP instead of 0.2 mM ATP. Since AMPPNP–Arp2/3 complex does not form branches (5), verified in our experiments (*SI Appendix*, Fig. S3), all branches formed from Arp2/3 complex with bound ATP. Since the flow buffer included 0.2 mM AMPPNP, all actin monomers remained bound to AMPNP. The solution with Arp2/3 complex accounted for less than 1% of the final solution volume, so it introduced a negligible amount of ATP.

In debranching experiments with GMF with or without BeF_x, samples were prepared as above except that debranching was initiated by gentle flow of buffer (15 μL·min^{-1}, very low force) containing a range of concentrations of GMF, and the flow was maintained throughout the experiment.

Data Analysis. Analysis of branch dissociation was done by manual tracking with ImageJ (https://imagej.nih.gov/). Branches that were fluctuating at all times and did not stick to the glass surface were selected randomly to minimize bias. These branches were labeled, cataloged, and observed for their entire lifetimes. Origin (https://www.originlab.com/) was used to fit all data and make plots. For the Arp2/3 complex debranching images in Fig. 1, a Gaussian blur with a sigma radius of 1.25 pixels was applied. Then images were background subtracted with a rolling ball radius of 15 pixels and subsequently contrast enhanced.

Data Availability. All protein purification protocols are referenced in *Materials and Methods*. Purification of GMF is described in *Materials and Methods*. Plasmid and the DNA sequence of GMF are provided in *SI Appendix, Part 4*. Details on movies for microscopy experiments are provided in *SI Appendix, Part 1*.

1. T. D. Pollard, J. A. Cooper, Actin, a central player in cell shape and movement. *Science* **326**, 1208–1212 (2009).
2. P. A. Janmey, C. A. McCulloch, Cell mechanics: Integrating cell responses to mechanical stimuli. *Annu. Rev. Biomed. Eng.* **9**, 1–34 (2007).
3. T. D. Pollard, Regulation of actin filament assembly by Arp2/3 complex and formins. *Annu. Rev. Biophys. Biomol. Struct.* **36**, 451–477 (2007).
4. C. Le Clainche, D. Didry, M. F. Carlier, D. Pantaloni, Activation of Arp2/3 complex by Wiskott-Aldrich Syndrome protein is linked to enhanced binding of ATP to Arp2. *J. Biol. Chem.* **276**, 46689–46692 (2001).
5. M. J. Dayel, E. A. Holleran, R. D. Mullins, Arp2/3 complex requires hydrolyzable ATP for nucleation of new actin filaments. *Proc. Natl. Acad. Sci. U.S.A.* **98**, 14871–14876 (2001).
6. L. Blanchoin, T. D. Pollard, R. D. Mullins, Interactions of ADF/cofilin, Arp2/3 complex, capping protein and profilin in remodeling of branched actin filament networks. *Curr. Biol.* **10**, 1273–1282 (2000).
7. M. J. Dayel, R. D. Mullins, Activation of Arp2/3 complex: Addition of the first subunit of the new filament by a WASP protein triggers rapid ATP hydrolysis on Arp2. *PLoS Biol.* **2**, E91 (2004).
8. E. Ingerman, J. Y. Hsiao, R. D. Mullins, Arp2/3 complex ATP hydrolysis promotes lamellipodial actin network disassembly but is dispensable for assembly. *J. Cell Biol.* **200**, 619–633 (2013).
9. C. Le Clainche, D. Pantaloni, M. F. Carlier, ATP hydrolysis on actin-related protein 2/3 complex causes debranching of dendritic actin arrays. *Proc. Natl. Acad. Sci. U.S.A.* **100**, 6337–6342 (2003).
10. A. C. Martin, M. D. Welch, D. G. Drubin, Arp2/3 ATP hydrolysis-catalysed branch dissociation is critical for endocytic force generation. *Nat. Cell Biol.* **8**, 826–833 (2006).
11. D. A. Fletcher, R. D. Mullins, Cell mechanics and the cytoskeleton. *Nature* **463**, 485–492 (2010).
12. L. Blanchoin, R. Boujemaa-Paterski, C. Sykes, J. Plastino, Actin dynamics, architecture, and mechanics in cell motility. *Physiol. Rev.* **94**, 235–263 (2014).
13. P. Bieling *et al.*, Force feedback controls motor activity and mechanical properties of self-assembling branched actin networks. *Cell* **164**, 115–127 (2016).
14. S. H. Parekh, O. Chaudhuri, J. A. Theriot, D. A. Fletcher, Loading history determines the velocity of actin-network growth. *Nat. Cell Biol.* **7**, 1219–1223 (2005).
15. J. Mueller *et al.*, Load adaptation of lamellipodial actin networks. *Cell* **171**, 188–200.e16 (2017).
16. R. E. Mahaffy, T. D. Pollard, Kinetics of the formation and dissociation of actin filament branches mediated by Arp2/3 complex. *Biophys. J.* **91**, 3519–3528 (2006).
17. R. E. Mahaffy, T. D. Pollard, Influence of phalloidin on the formation of actin filament branches by Arp2/3 complex. *Biochemistry* **47**, 6460–6467 (2008).
18. J. Berro, V. Sirotkin, T. D. Pollard, Mathematical modeling of endocytic actin patch kinetics in fission yeast: Disassembly requires release of actin filament fragments. *Mol. Biol. Cell* **21**, 2905–2915 (2010).
19. V. Sirotkin, J. Berro, K. Macmillan, L. Zhao, T. D. Pollard, Quantitative analysis of the mechanism of endocytic actin patch assembly and disassembly in fission yeast. *Mol. Biol. Cell* **21**, 2894–2904 (2010).
20. M. Gandhi *et al.*, GMF is a cofilin homolog that binds Arp2/3 complex to stimulate filament debranching and inhibit actin nucleation. *Curr. Biol.* **20**, 861–867 (2010).
21. B. L. Goode, M. O. Sweeney, J. A. Eskin, GMF as an actin network remodeling factor. *Trends Cell Biol.* **28**, 749–760 (2018).
22. C. A. Ydenberg *et al.*, GMF severs actin-Arp2/3 complex branch junctions by a cofilin-like mechanism. *Curr. Biol.* **23**, 1037–1045 (2013).
23. H. Kang *et al.*, Site-specific cation release drives actin filament severing by vertebrate cofilin. *Proc. Natl. Acad. Sci. U.S.A.* **111**, 17821–17826 (2014).
24. C. Chan, C. C. Beltzner, T. D. Pollard, Cofilin dissociates Arp2/3 complex and branches from actin filaments. *Curr. Biol.* **19**, 537–545 (2009).
25. G. I. Bell, Models for the specific adhesion of cells to cells. *Science* **200**, 618–627 (1978).
26. S. Rakshit, S. Sivasankar, Biomechanics of cell adhesion: How force regulates the lifetime of adhesive bonds at the single molecule level. *Phys. Chem. Chem. Phys.* **16**, 2211–2223 (2014).
27. A. Muhlrad, P. Cheung, B. C. Phan, C. Miller, E. Reisler, Dynamic properties of actin. Structural changes induced by beryllium fluoride. *J. Biol. Chem.* **269**, 11852–11858 (1994).

28. P. Ge, Z. A. O. Durer, D. Kudryashov, Z. H. Zhou, E. Reisler, Cryo-EM reveals different coronin binding modes for ADP- and ADP-BeFx actin filaments. *Nat. Struct. Mol. Biol.* **21**, 1075–1081 (2014).
29. M. F. Carlier, D. Pantaloni, Binding of phosphate to F-ADP-actin and role of F-ADP--Pi-actin in ATP-actin polymerization. *J. Biol. Chem.* **263**, 817–825 (1988).
30. L. A. Helgeson, B. J. Nolen, Mechanism of synergistic activation of Arp2/3 complex by cortactin and N-WASP. *eLife* **2**, e00884 (2013).
31. B. A. Smith, K. Daugherty-Clarke, B. L. Goode, J. Gelles, Pathway of actin filament branch formation by Arp2/3 complex revealed by single-molecule imaging. *Proc. Natl. Acad. Sci. U.S.A.* **110**, 1285–1290 (2013).
32. B. A. Smith *et al*., Three-color single molecule imaging shows WASP detachment from Arp2/3 complex triggers actin filament branch formation. *eLife* **2**, e01008 (2013).
33. A. C. Reymann *et al*., Actin network architecture can determine myosin motor activity. *Science* **336**, 1310–1314 (2012).
34. Sonal *et al*., Myosin-II activity generates a dynamic steady state with continuous actin turnover in a minimal actin cortex. *J. Cell Sci.* **132**, jcs219899 (2019).
35. C. A. Wilson *et al*., Myosin II contributes to cell-scale actin network treadmilling through network disassembly. *Nature* **465**, 373–377 (2010).
36. N. A. Medeiros, D. T. Burnette, P. Forscher, Myosin II functions in actin-bundle turnover in neuronal growth cones. *Nat. Cell Biol.* **8**, 215–226 (2006).
37. M. Vinzenz *et al*., Actin branching in the initiation and maintenance of lamellipodia. *J. Cell Sci.* **125**, 2775–2785 (2012).
38. L. M. McMillen, D. Vavylonis, Model of turnover kinetics in the lamellipodium: Implications of slow- and fast- diffusing capping protein and Arp2/3 complex. *Phys. Biol.* **13**, 66009 (2016).
39. T. Miyoshi *et al*., Actin turnover-dependent fast dissociation of capping protein in the dendritic nucleation actin network: Evidence of frequent filament severing. *J. Cell Biol.* **175**, 947–955 (2006).
40. K. Hayakawa, H. Tatsumi, M. Sokabe, Actin filaments function as a tension sensor by tension-dependent binding of cofilin to the filament. *J. Cell Biol.* **195**, 721–727 (2011).
41. D. E. Hannemann, W. Cao, A. O. Olivares, J. P. Robblee, E. M. De La Cruz, Magnesium, ADP, and actin binding linkage of myosin V: Evidence for multiple myosin V-ADP and actomyosin V-ADP states. *Biochemistry* **44**, 8826–8840 (2005).
42. E. V. Wong *et al*., Nup159 weakens Gle1 binding to Dbp5 but does not accelerate ADP release. *J. Mol. Biol.* **430**, 2080–2095 (2018).
43. M. Boczkowska, G. Rebowski, R. Dominguez, Glia maturation factor (GMF) interacts with Arp2/3 complex in a nucleotide state-dependent manner. *J. Biol. Chem.* **288**, 25683–25688 (2013).
44. K. Nakano, I. Mabuchi, Actin-depolymerizing protein Adf1 is required for formation and maintenance of the contractile ring during cytokinesis in fission yeast. *Mol. Biol. Cell* **17**, 1933–1945 (2006).
45. I. Rouiller *et al*., The structural basis of actin filament branching by the Arp2/3 complex. *J. Cell Biol.* **180**, 887–895 (2008).
46. B. R. McCullough, L. Blanchoin, J. L. Martiel, E. M. De la Cruz, Cofilin increases the bending flexibility of actin filaments: Implications for severing and cell mechanics. *J. Mol. Biol.* **381**, 550–558 (2008).
47. W. A. Elam *et al*., Phosphomimetic S3D cofilin binds but only weakly severs actin filaments. *J. Biol. Chem.* **292**, 19565–19579 (2017).
48. J. A. Cooper, S. B. Walker, T. D. Pollard, Pyrene actin: Documentation of the validity of a sensitive assay for actin polymerization. *J. Muscle Res. Cell Motil.* **4**, 253–262 (1983).
49. B. J. Nolen, T. D. Pollard, Structure and biochemical properties of fission yeast Arp2/3 complex lacking the Arp2 subunit. *J. Biol. Chem.* **283**, 26490–26498 (2008).
50. B. Y. Hua *et al*., An improved surface passivation method for single-molecule studies. *Nat. Methods* **11**, 1233–1236 (2014).
51. E. M. Johnson-Chavarria, U. Agrawal, M. Tanyeri, T. E. Kuhlman, C. M. Schroeder, Automated single cell microbioreactor for monitoring intracellular dynamics and cell growth in free solution. *Lab Chip* **14**, 2688–2697 (2014).
52. N. Courtemanche, J. Y. Lee, T. D. Pollard, E. C. Greene, Tension modulates actin filament polymerization mediated by formin and profilin. *Proc. Natl. Acad. Sci. U.S.A.* **110**, 9752–9757 (2013).
53. C. Brennen, H. Winet, Fluid-mechanics of propulsion by cilia and flagella. *Annu. Rev. Fluid Mech.* **9**, 339–398 (1977).
54. J. P. Robblee, W. Cao, A. Henn, D. E. Hannemann, E. M. De La Cruz, Thermodynamics of nucleotide binding to actomyosin V and VI: A positive heat capacity change accompanies strong ADP binding. *Biochemistry* **44**, 10238–10249 (2005).
55. E. W. Taylor, Kinetic studies on the association and dissociation of myosin subfragment 1 and actin. *J. Biol. Chem.* **266**, 294–302 (1991).

Force and phosphate release from Arp2/3 complex promote dissociation of actin filament branches

Authors: Nandan G. Pandit[a,d], Wenxiang Cao[a], Jeffrey Bibeau[a], Eric M. Johnson-Chavarria[a], Edwin W. Taylor[a], Thomas D. Pollard[a,b,c,d], Enrique M. De La Cruz[a,1]

[a] Department of Molecular Biophysics and Biochemistry, Yale University, New Haven, CT 06520
[b] Department of Molecular, Cellular, and Developmental Biology, Yale University, New Haven, CT 06520
[c] Department of Cell Biology, Yale University, New Haven, CT 06520
[d] Program in Physical and Engineering Biology, Yale University, New Haven, CT 06520
[1] Corresponding author (email: enrique.delacruz@yale.edu phone number: +1 (203) 432-5424)

Supplemental Information Appendix

Part 1. Supplementary figures and movies

Part 2. Two-state model for actin network debranching

Part 3. A model for the distribution of branches at the leading edge of cells based on the dependence of the rates of branch dissociation on age and applied force.

Part 4. DNA sequence of GMF

www.pnas.org/cgi/doi/10.1073/pnas.1911183117

Part 1. Supplementary figures and movies

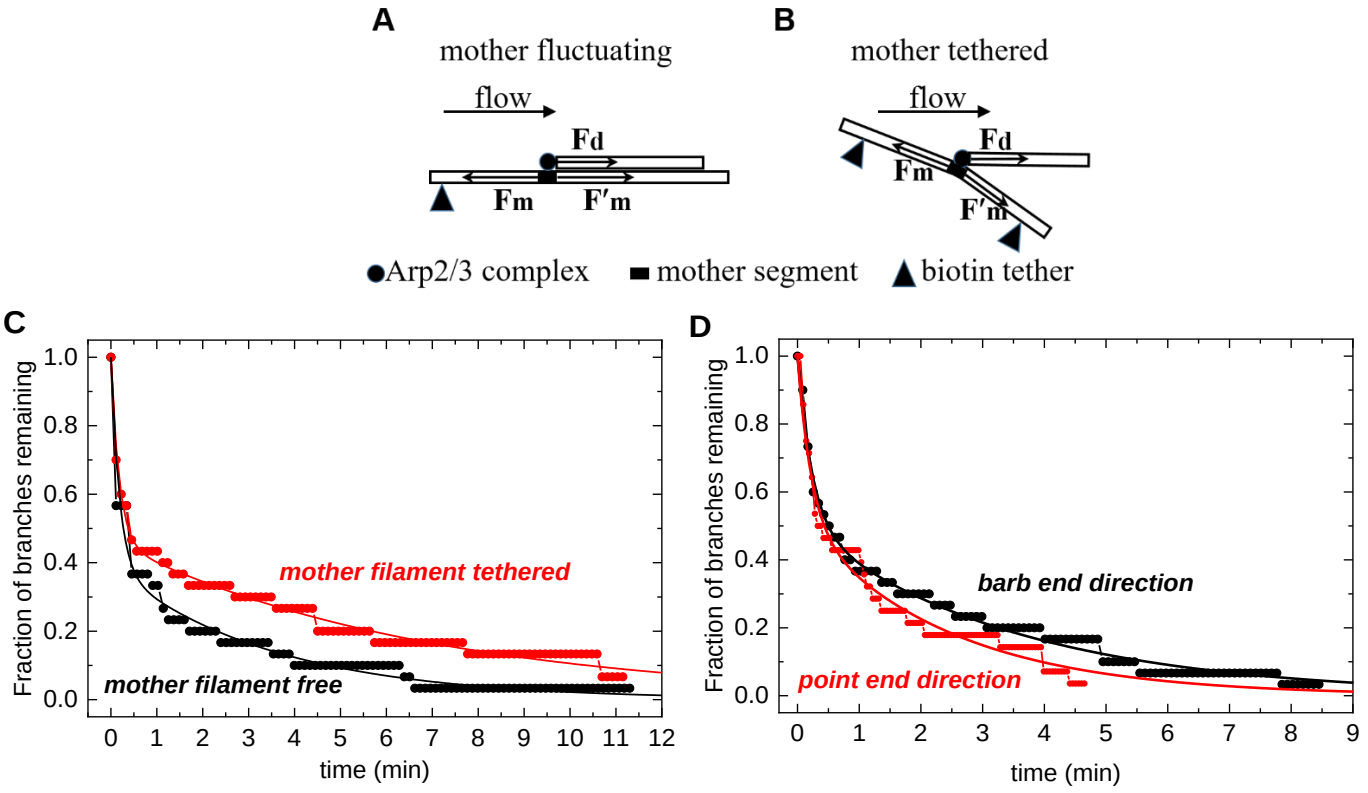

Fig. S1. Time courses of debranching depend weakly on tension in the mother filament and the direction of force. A and B. Free body diagram illustrating the forces acting on a mother filament segment (filled rectangular block) with a bound daughter filament. One force ($\mathbf{F_d}$) originates from pulling of the freely moving daughter filament. This force in the direction of flow scales with the daughter filament length and flow rate (Eq. 5). The other two forces originate from pulling of the flanking mother filament segments at each side ($\mathbf{F_m}$ and $\mathbf{F'_m}$) of the branch. For a freely fluctuating mother filament, $\mathbf{F_m}$ and $\mathbf{F'_m}$ align with the flow direction, but in opposite directions (A). When the entire mother filament is tethered, the orientations of $\mathbf{F_m}$ and $\mathbf{F'_m}$ are confined and do not align with flow. The amplitudes of $\mathbf{F_m}$ and $\mathbf{F'_m}$ vary with geometry (B). The tension induced in the mother filament segment with a branch must counter-balance all the three forces acting on it. C and D. Branched actin networks were assembled for ~4 min with the entire mother filament or just a pointed end segment tethered to the surface. Without additional aging, the time courses of debranching followed double exponentials (n = 30 branches) under 500 µL min^{-1} buffer flow (~1.02 pN of force for a branch of 1.5 µm). C. Time courses of branch dissociation from tethered and freely fluctuating mother filaments with the buffer flow at 500 µL min^{-1}. The smooth lines through data are the best double exponential fits, yielding fast phase lifetimes of 0.19 (±0.02; free) and 0.18 (±0.01; tethered) min, amplitudes of 18 vs. 16%, and slow phase lifetimes of 3.5 (±0.2; free) and 6.8 (±0.2; tethered) min. The uncertainties represent the standard deviations from the fits. The force on immobilized mother filaments depends on their (random) orientations, while freely-fluctuating mother filaments align with flow and experience tension in a single direction. Thirty branches were scored for both free and tethered mother filament conditions. D. Time courses of branch dissociation with the buffer flow at 500 µL min^{-1} towards the barbed or pointed ends of mother filaments oriented parallel to the direction of flow and tethered to the surface throughout their lengths. Flow toward the mother filament barbed end pushed branches "forward", while flow towards the mother filament pointed end pushed branches "backward". n =30 for the barbed end direction and n =28 for the pointed end. See Movie S6-7). The smooth lines through data are the best fits to double exponentials, yielding fast phase lifetimes of 0.23 (±0.02; barbed) and 0.22 (±0.02; pointed) min, amplitudes of 49 vs. 48%, and slow phase lifetimes of 3.5 (±0.1; barbed) and 2.4 (±0.1; pointed) min. The uncertainties represent the standard deviations from the fits.

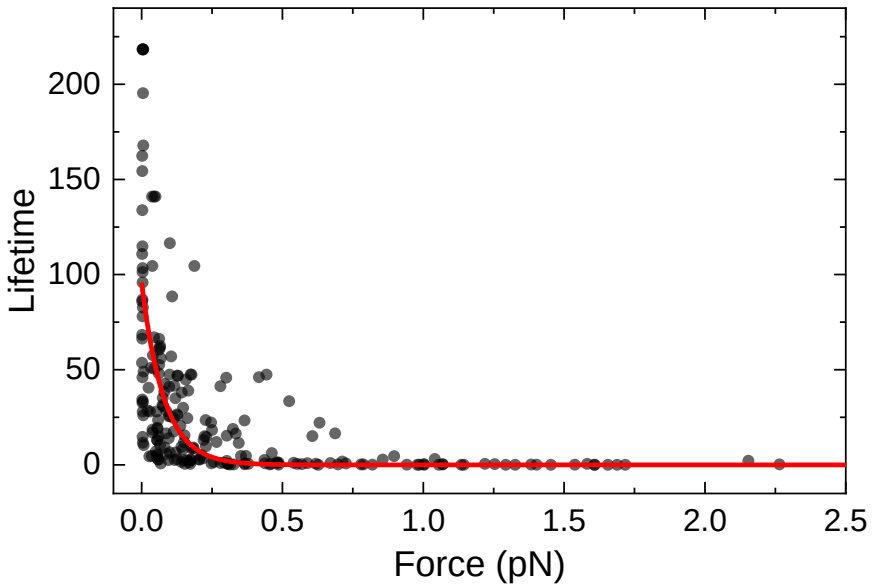

Fig. S2. (Previous Fig. 2D inset) Rug plot analysis of dependence of branch lifetimes on force for branches formed from ATP-Arp2/3 complex and aged for 30 min to form branches with ADP-Arp2/3 complex (time courses in Fig. 2A). Force dependence of individual branch lifetimes was fitted to Bell's equation (Eq. 1) for comparison. The best fit resulted in characteristic distance d = 52 (± 7) nm (F1/2 = 0.054 (± 0.008) pN) and branch lifetime with 0 force τ_0 = 96 (± 6) min (rate constant = τ_0^{-1} = 0.01 (± 0.007) min^{-1}).

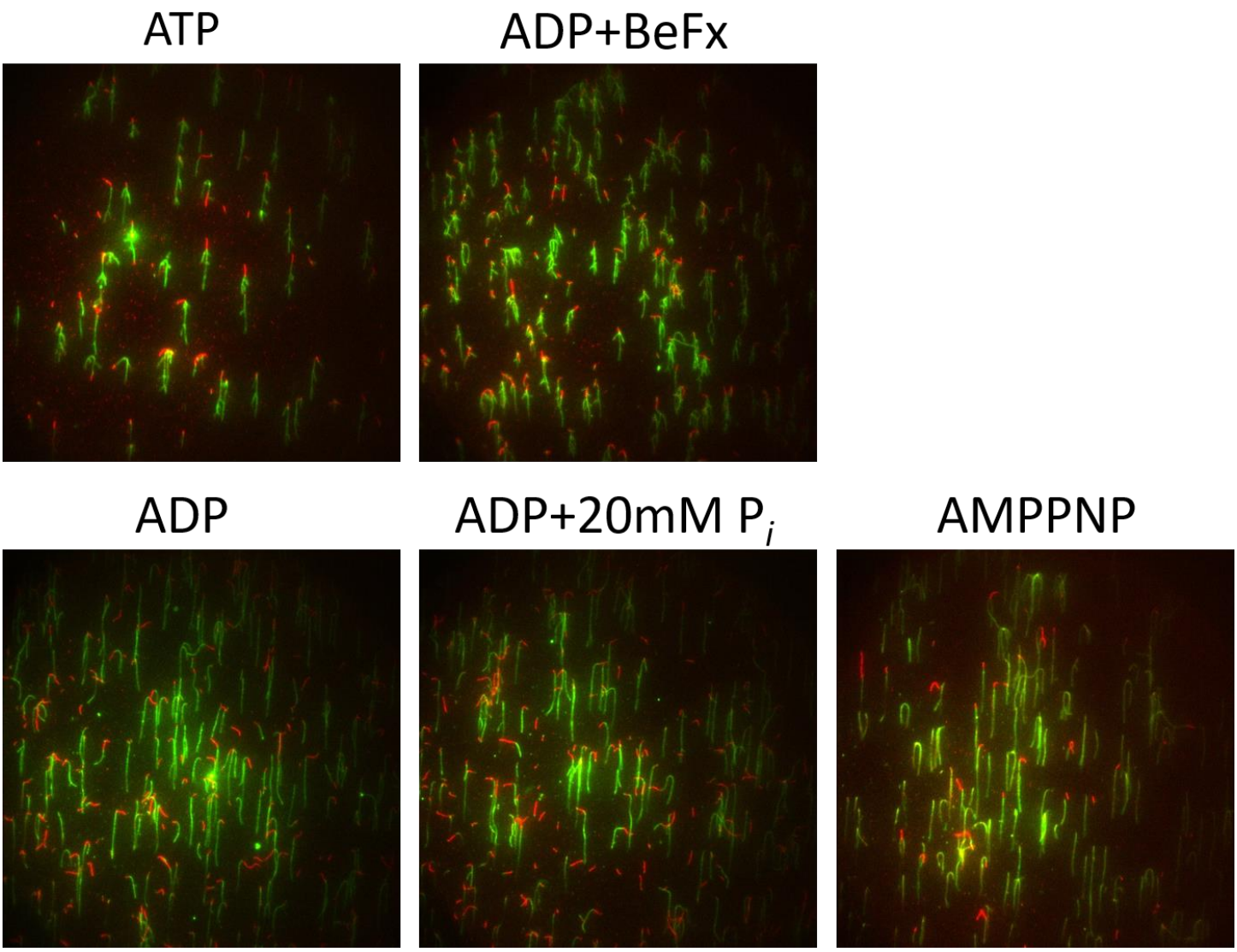

Fig. S3. Fluorescence micrographs of actin filaments in the presence of Arp2/3 complex in the flow chamber. Experimental set-up and fluorescent labeling are as described in Fig 1A. The flow rate is ≤25 μL min $^{-1}$. Upper row: ATP-actin and ATP-Arp2/3 complex (ATP) and ADP-actin ADP-BeF$_x$-Arp-2/3 complex (ADP+BeFx) prepared from ADP-Arp2/3 with 2 mM $BeSO_4$ + 10 mM NaF robustly form branches. Lower row: Neither ADP-actin and ADP-Arp2/3 complex, with or without 20 mM P_i (ADP, ADP+20 mM P_i), nor AMPPNP-actin and AMPPNP-Arp2/3 complex (AMPPNP) form branches under our experimental conditions.

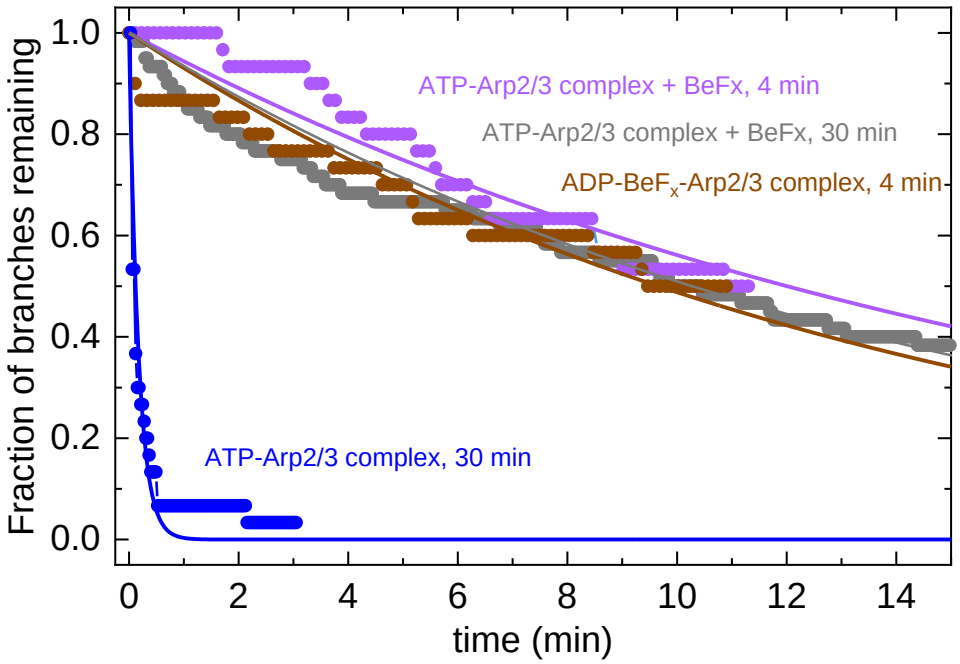

Fig. S4. Dissociation time courses of branches formed from ATP- or ADP-Arp2/3 complex in the presence or absence of BeF_x and aged for various times. Debranching was observed under force by applying 500 μL min^{-1} (approximately 1.02 pN for a branch of 1.5 μm). All time courses follow single exponentials with observed lifetimes of 0.21 (±0.02) min^{-1} for ATP-Arp2/3 complex aged for 30 min (blue), 13.9 (±0.2) min^{-1} for ADP-Arp2/3 complex in the presence of 2mM BeF_x and aged for ~4 min (brown), and 17.3 (±0.03) min^{-1} and 14.8 (±0.09) min^{-1} for branches formed with ATP-Arp2/3 complex in the presence of 2mM BeF_x and aged for ~4 min (purple) or 30 min (gray), respectively.

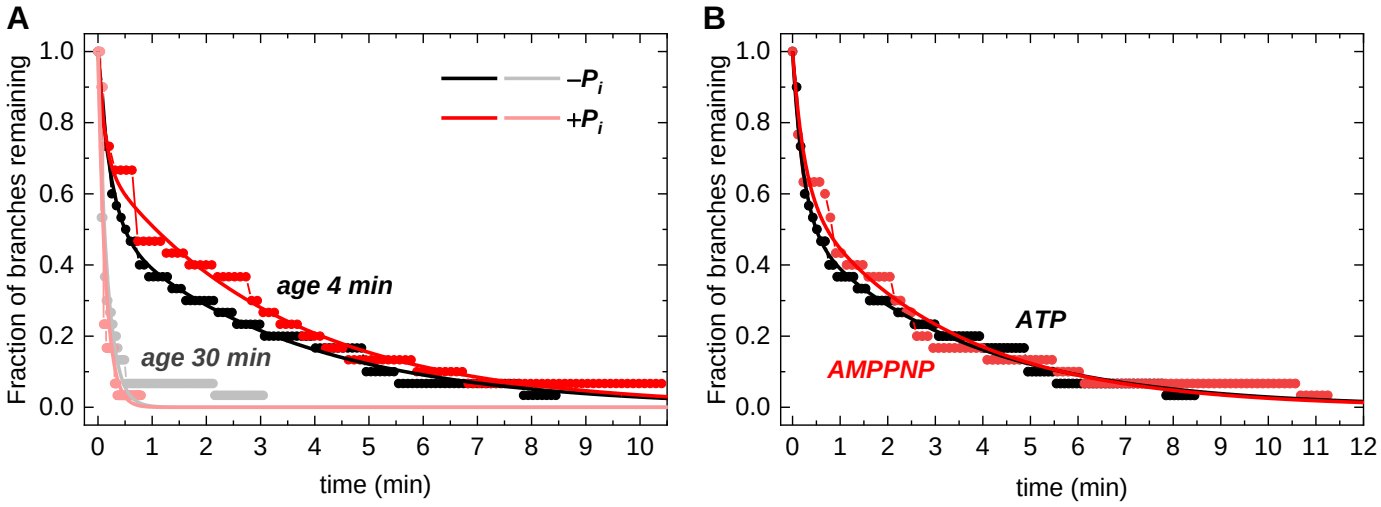

Fig. S5. The time course of debranching does not depend on the nucleotide state of the mother filament. (A) Comparison of the time courses of dissociation of branches assembled in polymerization buffer containing 0.2 mM ATP with 0 or 20 mM potassium phosphate and aged for ~4 min (dark colored traces) or 30 min (light colored traces) before observing the time course of branch dissociation at a buffer flow of 500 μL min^{-1} (approximately 1.02 pN of force for a branch of 1.5 μm). Phosphate (20 mM) saturates ADP-actin filaments to form ADP-P_i actin mother and daughter filaments. The affinity of ADP-Arp2 or Arp3 in branch junctions for phosphate is not known. *n* = 30 for all traces. The smooth lines through data are the best double exponential fits (~4 min aging, fast phase lifetime = 0.23 (±0.02; –P_i) and 0.12 (±0.02; +P_i) min, amplitude 0.47 vs. 0.3% and slow phase lifetime = 3.5 (±0.1; –P_i) and 3.3 (±0.1; +P_i) min) or single exponential (30 min aging; lifetime = 0.17 (±0.01; –P_i) and 0.14 (±0.01; +P_i) min). The uncertainties represent the standard deviations of the best fits of the data to single or double exponentials. (B) Comparison of the time courses of dissociation of branches assembled from ATP-Arp2/3 complex and ATP- or AMPPNP-actin monomers in polymerization buffer with 0.2 mM ATP or AMPPNP. After aging branches for ~4 min force was applied by buffer flowing at 500 μL min^{-1}. *n* = 30 branches for both conditions. The smooth lines through data are the best double exponential fits with slow phase lifetime of 3.5 (±0.1; ATP) vs. 3.2 (±0.1, AMPPNP) min and fast phase lifetime of 0.23 (±0.02; ATP) vs. 0.25 (±0.04, AMPPNP) min. The fast phase amplitude is 0.49 vs. 0.4%. The uncertainties represent the standard deviations of the best fits of the data to double exponentials.

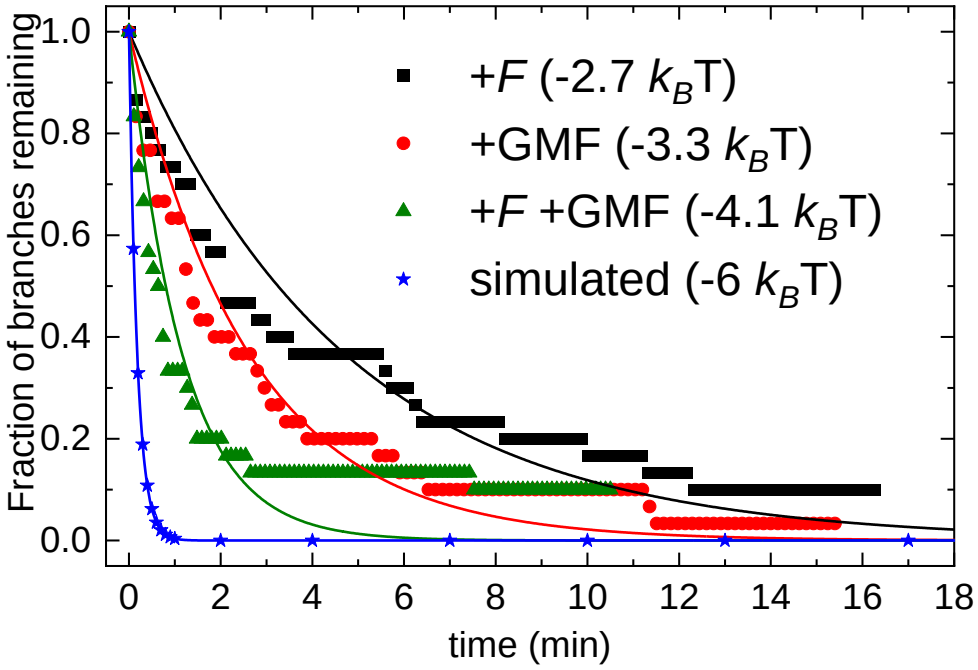

Fig. S6. Force and GMF together accelerate debranching of ADP-Arp2/3 complex branches more than either does alone. Branches were formed as described in *Methods* and aged for 30 min to form ADP-Arp2/3 complex branches. Debranching was then initiated with 15 (very weak force – approximately 0.03 pN for a 1.5 μm branch) or 125 μL min^{-1} (moderate force – approximately 0.25 pN for a 1.5 μm branch) flow with and without 500 nM GMF. Those time courses follow single exponential decays (Fig. 2A). Debranching of ADP-Arp2/3 complex branches under 125 μL min^{-1} flow was ~15-fold faster than under 15 μL min^{-1} flow (lifetime reduced from 71 to 4.7 min, filled black squares), corresponding to a reduction in debranching activation energy of 2.7 k_BT ($\Delta\Delta G^{\ddagger} = k_BT \ln(\tau_2/\tau_1)$. Inclusion of 500 nM GMF alone accelerated ADP-Arp2/3 complex branch debranching ~27 fold compared to that under weaker flow (15 μL min^{-1}) without GMF (lifetime from 71 to 2.6 min, filled red circles) and reduced the debranching activation energy by 3.3 k_BT. Force (125 μL min^{-1} flow) and GMF (500 nM) together further accelerate debranching of ADP-Arp2/3 complex branches, shortening the lifetime from 71 to 1.16 min (filled green triangles), corresponding to a reduction in debranching activation energy of 4.1 k_BT. This reduction in debranching activation energy less than the sum of 6 k_BT predicted if the effects of force and GMF were additive. A simulated debranching time course with an activation energy reduction of 6 k_BT with corresponding lifetime of 0.18 min is shown for comparison (filled blue stars). The uncertainties were propagated from standard deviation in the lifetime obtained from the best exponential fits.

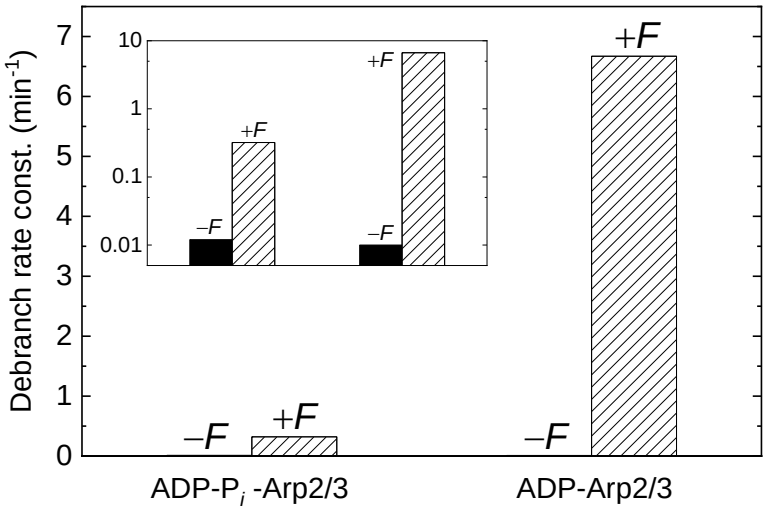

Fig. S7. Branches with ADP-Arp2/3 complex are far more sensitive to debranching by force than ADP-P$_i$-Arp2/3 complex. The debranching rate constants in the absence of force for ADP-P$_i$-Arp2/3 complex (k_1) and ADP-Arp2/3 branches (k_2) were determined from analysis of data in Figs. 2 and 4 (Table 1). The global double exponential fits of the aging time-dependence of debranching time courses (Fig. 2B) yielded the observed slow ($k_{s,F}$) and ($k_{f,F}$) phase rate constant under 500 μL min^{-1} flow force. The rate constant for ADP-Arp2/3 complex debranching under force ($k_{2,F}$) is the fast, observed rate constant (i.e. $k_{2,F} = k_{f,F}$), whereas the slow observed rate constant represents a composite of the rate constants for ADP-P$_i$-Arp2/3 complex debranching ($k_{1,F}$) and conversion ($k_{conv,F}$) under force (i.e. $k_{s,F} = k_{1,F} + k_{conv,F}$; Eq. S41). Accordingly, $k_{1,F}$ can be estimated as $k_1 \leq k_{1,F} < k_{s,F}$. The upper limit, where $k_{1,F} = k_{s,F}$, is plotted. The actual $k_{1,F}$ value under force is therefore smaller than plotted. Note that the y-axis of the inset is on a logarithmic scale.

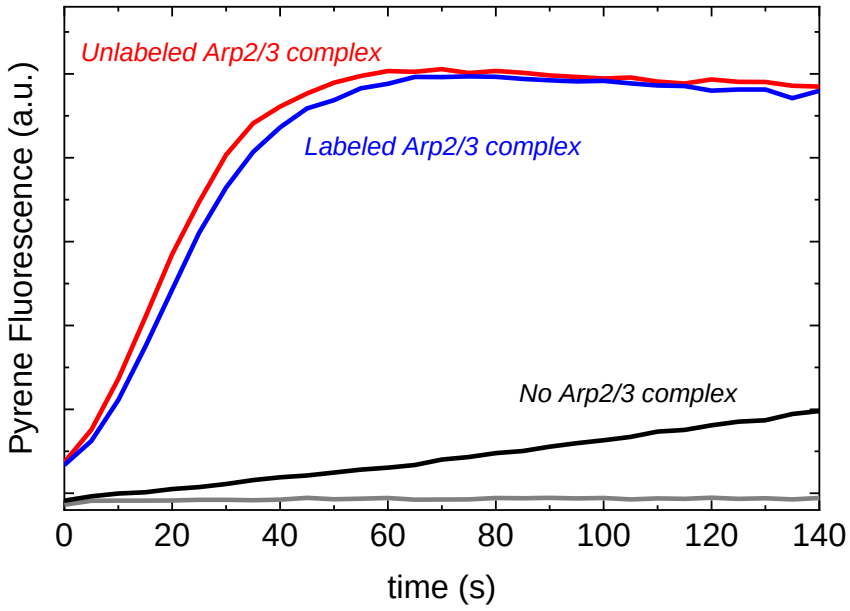

Fig S8. Comparison of the nucleation activity of Arp2/3 complex without a label and with Alexa-488 conjugated to a snap tag on the Arpc5 subunit monitored by the time course of pyrenyl-actin polymerization. Conditions: 3 µM actin monomers (30% pyrene labeled), 200 nM Arp2/3 complex (± 82% Alexa-488 labeled), and 500 nM GST-VCA at 25 °C. Reactants were mixed at time zero and fluorescence emission was recorded at 407 nm (excitation wavelength = 365 nm) in a plate reader (Molecular Devices, SpectraMax GEMINI XPS). Red curve: unlabeled Arp2/3 complex in KMIE polymerization buffer; Blue curve: Alexa-488 Snap ArpC5 Arp2/3 complex in KMIE polymerization buffer; Black curve: 30% labeled pyrene monomers alone (no Arp2/3 complex) in KMIE polymerization buffer; Grey curve: 30% labeled pyrene actin monomers alone in low salt, non-polymerizing, G-buffer (1).

Videos

Time lapse movies of fluorescence micrographs at different frame rates and flow rates showing dissociation of a branches formed by Arp2/3 complex. Filament seeds containing 15% 568-Alexa and 10% biotin were incubated with 1.5μM of 15% 647-Alexa ATP-actin monomers, 100 nM ATP-Arp2/3 complex, and 500 nM GST-VCA in KMIE buffer for 1 to 2 minutes at 25 °C then immobilized on the neutravidin coated glass surface (*Materials and Methods*). Unbound proteins were washed out with KMIE buffer supplemented with 0.2 μM unlabeled actin monomers, 15 mM glucose, 0.02 mg mL^{-1} catalase, and 0.1 mg mL^{-1} glucose oxidase. In these movies, the filaments were aged for 30 min to form ADP-actin filaments and ADP-Arp2/3 complex then KMIE buffer supplemented with 0.2 μM unlabeled actin monomers, 15 mM glucose, 0.02 mg mL^{-1} catalase, and 0.1 mg mL^{-1} glucose oxidase flow was applied at a constant but variable rate throughout the entire movie. The videos begin after aging and before applying flow (flow rate is specified in each caption). The flow is applied towards the mother filament barbed end direction (bottom to top of the image). In videos S1-3, S6, and S7, the red or magenta portion of the actin filament is immobilized on the surface with biotin whereas the green or cyan portion of the actin filament (mother filament or branch) is freely fluctuating (Fig. 1A). In videos S4 and S5, the entire mother filament is colored red or magenta and the 488-Alexa labeled Arp2/3 complex is colored green or cyan. The scale bars represent 2 μm. The samples are stationary but appear to drift due to imprecise repositioning of the stage as it moved continuously to capture multiple fields of view during the experiments.

Movie S1: Time lapse movies of fluorescence micrographs at 20 s intervals showing dissociation of a branch formed by Arp2/3 complex at time 1680 s with a flow rate of 2 μL min^{-1}, corresponding to a “low” force of ~0.004 pN on a branch 1.5 μm long.

Movie S2: Time lapse movies of fluorescence micrographs at 10 s intervals showing dissociation of a branch formed by Arp2/3 complex at time 1050 s with a flow rate of 50 μL min^{-1}, corresponding to a “medium” force of ~0.10 pN on a branch 1.5 μm long.

Movie S3: Time lapse movies of fluorescence micrographs at 3s intervals showing dissociation of a branch formed by Arp2/3 complex at time 48, 66, 219, and 480 s with a flow rate of 500 μL min^{-1}, corresponding to a “medium” force of ~1.02 pN on a branch 1.5 μm long.

Movie S4 and 5: Time lapse movies of fluorescence micrographs at 100 ms intervals showing dissociation of a branch formed by 488-Alexa labeled snap Arp2/3 complex at approximately 5 s (denoted by the white arrow) with a flow rate of 500 μL min^{-1}, corresponding to a “high” force of ~1.02 pN on a branch 1.5 μm long. Buffer flow is applied after 300 ms, 3 frames.

Movie S6: Time lapse movies of fluorescence micrographs at 3 s intervals showing dissociation of a branch formed by Arp2/3 complex that are aligned with the direction of buffer flow at time 33, 39, 54 s with a flow rate of 500 μL min^{-1}, corresponding to a “high” force of ~1.02 pN on a branch 1.5 μm long.

Movie S7: Time lapse movies of fluorescence micrographs at 3 s intervals showing dissociation of a branch formed by Arp2/3 complex that are aligned against the direction of buffer flow at time 36, 90 s with a flow rate of 500 μL min^{-1}, corresponding to a “high” force of ~1.02 pN on a branch 1.5 μm long.

Part 2. Two-state model for actin network debranching.

Actin network debranching was interpreted using the following branched kinetic pathway model (Scheme S1; Figure 2B) containing two Arp2/3 complex (*Arp*) mechanical states that convert irreversibly with rate constant k_{conv} and dissociate independently from the mother filament (*A*) with rate constants k_1 and k_2:

$$\begin{array}{ccccc} Arp + A & \xrightarrow{k_{form}} & branch_1 & \xrightarrow{k_{conv}} & branch_2 \\ & & \downarrow k_1 & & \downarrow k_2 \\ & & debranched & & \end{array} \qquad \text{Scheme S1}$$

The derivation and analysis presented here were used to determine the rate constants for branch formation (k_{form}), conversion between mechanical state 1 and 2 (k_{conv}), and debranching (k_1 and k_2).

Our experiments were carried out under two distinct force and reaction component regimes: all protein components were mixed together and the branched network was allowed to form for 2.6 min in KMIE buffer containing 2 mM MgATP, after which free unreacted protein and other components (e.g. labeled actin monomer, Arp2/3 complex, GST-VCA and other proteins, as indicated) were washed out by gentle flow of the same KMIE buffer containing 0.2 μM unlabeled actin monomer to prevent filaments from depolymerization. Without free Arp2/3 complex in solution, no additional branches formed after this initial washout. Branched networks were then allowed to further "age" for various times (with gentle flow of 2 μL min^{-1}; force ≈ 0 to minimize any rebinding of dissociating protein components) before applying constant external force with flow.

During filament assembly and aging, polymerized actin hydrolyzes bound ATP with a rate constant of 0.3 sec^{-1} and releases the γ-phosphate slowly (2, 3). Arp2 and Arp3 also hydrolyze bound ATP and dissociate γ-phosphate after branch formation (4, 5). Debranching was observed under flow, so debranched filaments were washed away and branch dissociation was considered to be irreversible. External force can affect k_{conv}, k_1 and/or k_2. Force may also influence branch formation and the value of k_{form}, but we assembled branches in the absence of force.

1) <u>*Minimal model for two Arp2/3 nucleotide branch formation without force during aging time*</u>.
Arp2/3 complex with ATP bound to Arp2 and Arp3 binds actin filaments. Only ~1% of binding events are productive and generate branches (6). We combine reversible Arp2/3 binding and subsequent irreversible branch formation into a single irreversible branch formation step, defined as composite association rate constant k_{form} (Scheme 1). We note that branch formation and dissociation occur through different reaction pathways, rather than a single reversible reaction.

Immediately after branch formation, Arp2/3 complexes are in state 1 ($branch_1$) which we assume is the ADP-P_i state, since ATP hydrolysis is coupled to branch formation ((4), see also (5)). If hydrolysis lags slightly after formation, as with actin (7), $branch_1$ could represent a mixture of ATP and ADP-P_i states. State 1 branches can elongate, dissociate irreversibly with rate constant k_1, or convert to state 2 ($branch_2$) with rate constant k_{conv}. The conversion from state 1 to state 2 is likely associated with P_i release from Arp2/3 complex (discussed in main text). Therefore, the conformation of the Arp2/3 complex in state 1 is considered an ADP-P_i conformation/state, whereas state 2 an ADP conformation/state. Conversion is treated as an (essentially) irreversible transition, given that inclusion of 20 mM P_i has no detectable effects on debranching (Figure S2). This behavior could arise from an irreversible kinetic transition associated with P_i release (since released P_i is washed away and cannot rebind) and/or a weak P_i binding affinity (K_d >> 20 mM).

Given these conditions, the differential equations describing the biochemical reactions depicted in Scheme 1 are given by:

$$\frac{d[branch_1]}{dt} = k_{form}[Arp][A] - \left(k_{conv} + k_1\right)[branch_1]$$
$$= k_{form}[Arp]\left([A]_0 - [branch_1] - [branch_2]\right) - \left(k_{conv} + k_1\right)[branch_1]$$

$$= k_{form}[Arp][A]_0 - \left(k_{form}[arp] + k_{conv} + k_1\right)[branch_1] - k_{form}[Arp][branch_2] \quad \text{S1}$$

and

$$\frac{d[branch_2]}{dt} = k_{conv}[branch_1] - k_2[branch_2], \quad \text{S2,}$$

where $[A]$ is the concentration of filamentous actin available (i.e. free) to bind Arp2/3 complex, while $[A]_0$ is total filamentous actin concentration (free and with bound Arp 2/3 complex). Mass conservation dictates that $[A]_0 = [A] + [branch_1] + [branch_2]$.

The Eigen values of Eqs. S1 and S2 yield two observed rate constants (λ_1 and λ_2) according to:

$$\begin{vmatrix} k_{form}[Arp] + k_{conv} + k_1 - \lambda & k_{form}[Arp] \\ -k_{conv} & k_2 - \lambda \end{vmatrix} = \left(k_{form}[Arp] + k_{conv} + k_1 - \lambda\right)\left(k_2 - \lambda\right) + k_{conv}k_{form}[Arp] \quad \text{S3,}$$

And its characteristic equation is

$$\lambda^2 - \left(k_{form}[Arp] + k_{conv} + k_1 + k_2\right)\lambda + k_2\left(k_{form}[Arp] + k_{conv} + k_1\right) + k_{conv}k_{form}[Arp] = 0 \quad \text{S4,}$$

The two exponential rate constants ($\lambda_{form,+/-}$) for branch formation are given by:

$$\lambda_{form,\pm} = \frac{1}{2}\left(k_{form}[Arp] + k_{conv} + k_1 + k_2 \right.$$
$$\left. \pm\sqrt{\left(k_{form}[Arp] + k_{conv} + k_1 + k_2\right)^2 - 4\left(k_2\left(k_{form}[Arp] + k_{conv} + k_1\right) + k_{conv}k_{form}[Arp]\right)}\right). \quad \text{S5.}$$

To obtain a constant special solution for the differential equations Eqs. S1 and S2, we let $[branch_1] = C_1$ and $[branch_2] = C_2$ and substitute them into Eqs. S1 and S2 to yield:

$$\frac{dC_1}{dt} + \left(k_{form}[Arp] + k_{conv} + k_1\right)C_1 + k_{form}[Arp]C_2$$
$$= \left(k_{form}[Arp] + k_{conv} + k_1\right)C_1 + k_{form}[Arp]C_2 = k_{form}[Arp][A]_0$$
$$-k_2C_1 + \frac{dC_2}{dt} + k_2C_2 = -k_2C_1 + k_2C_2 = 0 \quad \text{S6.}$$

The solution to these differential equations is given by:

$$C_1 = \frac{\begin{vmatrix} k_{form}[Arp][A]_0 & k_{form}[Arp] \\ 0 & k_2 \end{vmatrix}}{\begin{vmatrix} k_{form}[Arp] + k_{conv} + k_1 & k_{form}[Arp] \\ -k_{conv} & k_2 \end{vmatrix}} = \frac{k_2k_{form}[Arp][A]_0}{k_2\left(k_{form}[arp] + k_{conv} + k_1\right) + k_{conv}k_{form}[Arp]} \quad \text{S7}$$

and

$$C_2 = \frac{\begin{vmatrix} k_{form}[Arp] + k_{conv} + k_1 & k_{form}[Arp][A]_0 \\ -k_{conv} & 0 \end{vmatrix}}{\begin{vmatrix} k_{form}[Arp] + k_c + k_1 & k_{form}[Arp] \\ -k_{conv} & k_2 \end{vmatrix}} = \frac{k_ck_{form}[Arp][A]_0}{k_2\left(k_{form}[Arp] + k_{conv} + k_1\right) + k_{conv}k_{form}[Arp]} \quad \text{S8.}$$

Eqs. S1 and S2 have the following general solution:

$$\begin{pmatrix}[branch_1]\\ [branch_2]\end{pmatrix} = A_{form,+}\begin{pmatrix}1\\ \dfrac{k_{conv}}{k_2-\lambda_{form,+}}\end{pmatrix}e^{-\lambda_{form,+}t} + A_{form,-}\begin{pmatrix}1\\ \dfrac{k_{conv}}{k_2-\lambda_{form,-}}\end{pmatrix}e^{-\lambda_{form,-}t}$$
$$+\frac{k_{form}[Arp][A]_0}{k_2\left(k_{form}[Arp]+k_{conv}+k_1\right)+k_{conv}k_{form}[Arp]}\begin{pmatrix}k_2\\ k_{conv}\end{pmatrix}$$
$$= A_{form,+}\begin{pmatrix}1\\ \dfrac{k_{conv}}{k_2-\lambda_{form,+}}\end{pmatrix}e^{-\lambda_{form,+}t} + A_{form,-}\begin{pmatrix}1\\ \dfrac{k_{conv}}{k_2-\lambda_{form,-}}\end{pmatrix}e^{-\lambda_{form,-}t} + q\begin{pmatrix}k_2\\ k_{conv}\end{pmatrix} \quad \text{S9,}$$

where the constant q in the third term is defined as

$$q = \frac{k_{form}[Arp][A]_0}{k_2\left(k_{form}[Arp]+k_{conv}+k_1\right)+k_{conv}k_{form}[Arp]} \quad \text{S10.}$$

$A_{form,+}$ and $A_{form,-}$ in Eq. S9 are arbitrary amplitude constants that depend on the branch concentration and thus, protein concentration. We assume that no branches exist at $t = 0$:

$$\left.\begin{pmatrix}[branch_1]\\ [branch_2]\end{pmatrix}\right|_{t=0} = A_{form,+}\begin{pmatrix}1\\ \dfrac{k_{conv}}{k_2-\lambda_{form,+}}\end{pmatrix} + A_{form,-}\begin{pmatrix}1\\ \dfrac{k_{conv}}{k_2-\lambda_{form,-}}\end{pmatrix} + q\begin{pmatrix}k_2\\ k_{conv}\end{pmatrix}$$
$$= \begin{pmatrix}A_{form,+}+A_{form,-}+k_2 q\\ \dfrac{A_{form,+}k_{conv}}{k_2-\lambda_{form,+}} + \dfrac{A_{form,-}k_{conv}}{k_2-\lambda_{form,-}} + k_c q\end{pmatrix} = \begin{pmatrix}0\\ 0\end{pmatrix} \quad \text{S11.}$$

Solving Eq. S11, the constants are given by the following:

$$A_{+\,form,} = q\frac{\begin{vmatrix}-k_2 & 1\\ -1 & \dfrac{1}{k_2-\lambda_{form,-}}\end{vmatrix}}{\begin{vmatrix}1 & 1\\ \dfrac{1}{k_2-\lambda_{form,+}} & \dfrac{1}{k_2-\lambda_{form,-}}\end{vmatrix}} = q\frac{-\dfrac{k_2}{k_2-\lambda_{form,-}}+1}{\dfrac{1}{k_2-\lambda_{form,-}}-\dfrac{1}{k_2-\lambda_{form,+}}} = q\frac{-\lambda_{form,-}\left(k_2-\lambda_{form,+}\right)}{-\lambda_{form,+}+\lambda_{form,-}} \quad \text{S12,}$$

and

$$A_{form,-} = q\frac{\begin{vmatrix} 1 & -k_2 \\ \dfrac{1}{k_2-\lambda_{form,+}} & -1 \end{vmatrix}}{\begin{vmatrix} 1 & 1 \\ \dfrac{1}{k_2-\lambda_{form,+}} & \dfrac{1}{k_2-\lambda_{form,-}} \end{vmatrix}} = q\frac{-1+\dfrac{k_2}{k_2-\lambda_{form,+}}}{\dfrac{1}{k_2-\lambda_{form,-}}-\dfrac{1}{k_2-\lambda_{form,+}}} = q\frac{\lambda_{form,+}\left(k_2-\lambda_{form,-}\right)}{-\lambda_{form,+}+\lambda_{form,-}} \quad \text{S13,}$$

and the solution to Eq. S9 is given by:

$$\begin{pmatrix}[branch_1]\\ [branch_2]\end{pmatrix} = q\frac{-\lambda_{form,-}\left(k_2-\lambda_{form,+}\right)}{-\lambda_{form,+}+\lambda_{form,-}}\begin{pmatrix}1\\ \dfrac{k_{conv}}{k_2-\lambda_{form,+}}\end{pmatrix}e^{-\lambda_{form,+}t}$$

$$+q\frac{\lambda_{form,+}\left(k_2-\lambda_{form,-}\right)}{-\lambda_{form,+}+\lambda_{form,-}}\begin{pmatrix}1\\ \dfrac{k_{conv}}{k_2-\lambda_{form,-}}\end{pmatrix}e^{-\lambda_{form,-}t}+q\begin{pmatrix}k_2\\ k_{conv}\end{pmatrix}$$

$$=q\begin{pmatrix}-\dfrac{\lambda_{form,-}\left(k_2-\lambda_{form,+}\right)}{-\lambda_{form,+}+\lambda_{form,-}}e^{-\lambda_{form,+}t}+\dfrac{\lambda_{form,+}\left(k_2-\lambda_{form,-}\right)}{-\lambda_{form,+}+\lambda_{form,-}}e^{-\lambda_{form,-}t}+k_2\\ \dfrac{k_{conv}}{-\lambda_{form,+}+\lambda_{form,-}}\left(-\lambda_{form,-}e^{-\lambda_{form,+}t}+\lambda_{form,+}e^{-\lambda_{form,-}t}\right)+k_{conv}\end{pmatrix} \quad \text{S14.}$$

2) *Model for converting between Arp2/3 actin branch nucleotide states under no force during aging.*
After initial branched actin filament network formation, all untethered proteins (free actin, Arp2/3 complex, and GST-VCA) are washed out of the reaction chamber so that no additional branches form. Accordingly, the relevant reaction scheme during the remaining aging time after wash out should be identical to Scheme S1 without the branch formation transition:

$$\begin{array}{ccc} branch_1 & \xrightarrow{k_{conv}} & branch_2 \\ \downarrow k_1 & & \downarrow k_2 \\ debranched & & \end{array} \quad \text{Scheme S2}$$

The differential equations describing the reactions in Scheme S2 are:

$$\frac{d[branch_1]}{dt} = -\left(k_1+k_{conv}\right)[branch_1] \quad \text{S15}$$

$$\frac{d[branch_2]}{dt} = k_{conv}[branch_1]-k_2[branch_2] \quad \text{S16.}$$

Note that the differential equation accounting for *branch*$_2$ formation (Eq. S16) following Scheme S2 is identical to that obtained according to Scheme S1 (Eq. S2).

Differential equation Eq. S15 can be directly integrated to yield:

$$[branch_1] = [branch_1]_{t_1}e^{-(k_{conv}+k_1)(t-t_1)} \quad \text{S17,}$$

where $[branch_1]_{t_1}$ is the concentration of branches in the *branch*$_1$ state formed during time t_1. Substituting Eq. S17 into Eq. S16 yields

$$\frac{d[branch_2]}{dt} + k_2[branch_2] = k_{conv}[branch_1]_{t_1} e^{-(k_{conv}+k_1)(t-t_1)} \quad \text{S18.}$$

Using the variation of parameter method, a general solution of this inhomogeneous differential equation (Eq. S18) can be obtained. When $k_2 \neq k_1 + k_{conv}$:

$$[branch_2] = \frac{k_{conv}[branch_1]_{t_1}}{k_2 - k_1 - k_{conv}} e^{-(k_1+k_{conv})(t-t_1)} + Ce^{-k_2(t-t_1)}, \quad k_2 \neq k_1 + k_{conv} \quad \text{S19,}$$

and when $k_2 = k_1 + k_{conv}$:

$$[branch_2] = \left(k_{conv}[branch_1]_{t_1} t + C\right) e^{-k_2(t-t_1)}, \quad k_2 = k_1 + k_{conv} \quad \text{S20.}$$

Eqs. S17, S19 and S20 show that when $k_2 \neq k_1 + k_{conv}$, the debranching process has two exponential phases (given by Eqs. S17 and S19) with observed rate constants ($k_{obs,1}$ and $k_{obs,2}$) defined by ($k_1 + k_{conv}$) and k_2, respectively. When $k_2 = k_1 + k_{conv}$, the debranching process is sum of a single exponential ($k_{obs} = (k_1 + k_{conv})$ or k_2) and a non-exponential phase (Eqs. S17 and S20).

The arbitrary constant C in Eqs. S19 and S20 is determined by the populations of $branch_1$ and $branch_2$ formed during formation time t_1. When $t = t_1$, the constant C in Eqs. S19 and S20 is given by:

$$C = [branch_2]_{t_1} - \frac{k_{conv}[branch_1]_{t_1}}{k_2 - k_1 - k_{conv}}, \quad k_2 \neq k_1 + k_{conv} \quad \text{S21}$$

or

$$C = [branch_2]_{t_1} - k_{conv}[branch_1]_{t_1} t_1, \quad k_2 = k_1 + k_{conv} \quad \text{S22.}$$

Substituting of Eq. S21 or S22 into Eq. S19 or S20 generates:

$$[branch_2] = \frac{k_{conv}[branch_1]_{t_1}}{k_2 - k_1 - k_{conv}} e^{-(k_1+k_{conv})(t-t_1)} + \left([branch_2]_{t_1} - \frac{k_{conv}[branch_1]_{t_1}}{k_2 - k_1 - k_{conv}}\right) e^{-k_2(t-t_1)} \quad \text{S23}$$

$$k_2 \neq k_1 + k_{conv}$$

and

$$[branch_2] = \left(k_{conv}[branch_1]_{t_1} t + [branch_2]_{t_1} - k_{conv}[branch_1]_{t_1} t_1\right) e^{-k_2(t-t_1)}$$

$$= \left(k_{conv}[branch_1]_{t_1} (t - t_1) + [branch_2]_{t_1}\right) e^{-k_2(t-t_1)}, \quad k_2 = k_1 + k_{conv} \quad \text{S24.}$$

Therefore, the time dependent total combined branches in two states is the sum of Eqs. S17 and S23 or S24

$$[branch_1] + [branch_2] = [branch_1]_{t_1} e^{-(k_{conv}+k_1)(t-t_1)} + \frac{k_{conv}[branch_1]_{t_1}}{k_2 - k_1 - k_{conv}} e^{-(k_1+k_{conv})(t-t_1)}$$

$$+ \left([branch_2]_{t_1} - \frac{k_{conv}[branch_1]_{t_1}}{k_2 - k_1 - k_{conv}}\right) e^{-k_2(t-t_1)}$$

$$= \frac{(k_2 - k_1)[branch_1]_{t_1}}{k_2 - k_1 - k_{conv}} e^{-(k_1+k_{conv})(t-t_1)} + \left([branch_2]_{t_1} - \frac{k_{conv}[branch_1]_{t_1}}{k_2 - k_1 - k_{conv}}\right) e^{-k_2(t-t_1)} \quad \text{S25}$$

$$k_2 \neq k_1 + k_{conv}$$

or

$$[branch_1] + [branch_2] = [branch_1]_{t_1} e^{-(k_{conv}+k_1)(t-t_1)} + \left(k_{conv}[branch_1]_{t_1} (t - t_1) + [branch_2]_{t_1}\right) e^{-k_2(t-t_1)} \quad \text{S26.}$$

$$k_2 = k_1 + k_{conv}$$

If $k_1 \sim k_2$, the first exponential term in Eq. 25 disappears and the combined total branches of two states follow a single exponential decay (see below).

3) *Model for Arp2/3 actin branches debranching under force after aging*.
After a defined aging time t_{age} (accounted in the two preceding sections), dynamic flow was introduced to exert drag force on branches. The applicable reaction scheme under these experimental conditions is identical to that illustrated in Scheme S2, but with all rate constants replaced with ones under force (k_1, k_2 and k_{conv} become $k_{1,F}$, $k_{2,F}$ and $k_{conv,F}$). Accordingly, debranching under force follows the equations in the same form as Eqs. S17 and S23:

$$[branch_1]_F = [branch_1]_{F,0} e^{-(k_{conv,F}+k_{1,F})t} \quad \text{S27}$$

$$[branch_2]_F = \frac{k_{conv,F}[branch_1]_{F,0}}{k_{2,F}-k_{1,F}-k_{conv,F}} e^{-(k_{1,F}+k_{conv,F})t} + \left([branch_2]_{F,0} - \frac{k_{conv,F}[branch_1]_{F,0}}{k_{2,F}-k_{1,F}-k_{conv,F}} \right) e^{-k_{2,F}t} \quad \text{S28.}$$

$$k_{2,F} \neq k_{1,F} + k_{conv,F}$$

Because time courses of debranching under force follow a sum of exponentials, we can eliminate the solution with $k_{2,F} = k_{1,F} + k_{conv,F}$ (S24) since this has a non-exponential term in it that is not observed in the experimental data.

Time courses of observed debranching under force is given by sum of debranching from the both Arp2/3 complex branch states:

$$\begin{aligned}[branch]_F &= [branch_1]_{F,0} e^{-(k_{conv,F}+k_{1,F})t} + \frac{k_{conv,F}[branch_1]_{F,0}}{k_{2,F}-k_{1,F}-k_{conv,F}} e^{-(k_{1,F}+k_{conv,F})t} \\ &+ \left([branch_2]_{F,0} - \frac{k_{c,F}[branch_1]_{F,0}}{k_{2,F}-k_{1,F}-k_{conv,F}} \right)_F e^{-k_{2,F}t} \\ &= \frac{(k_{2,F}-k_{1,F})[branch_1]_{F,0}}{k_{2,F}-k_{1,F}-k_{conv,F}} e^{-(k_{1,F}+k_{conv,F})t} + \left([branch_2]_{F,0} - \frac{k_{conv,F}[branch_1]_{F,0}}{k_{2,F}-k_{1,F}-k_{conv,F}} \right) e^{-k_{2,F}t} \end{aligned} \quad \text{S29.}$$

Time courses of debranching follow double exponentials with slow (s) and fast (f) observed rate constants (k_s and k_f) equal to ($k_{1,F} + k_{conv,F}$) and $k_{2,F}$. The experimental data shows that aging accelerates branch dissociation (Figure 3). Therefore, fast dissociation occurs late in Scheme S2 and $k_s = (k_{1,F} + k_{conv,F})$ and $k_f = k_{2,F}$.

We define $[branch_1]_{F,0}$ and $[branch_2]_{F,0}$ as initial branch populations (formed during aging in the absence of force) the moment that force is applied. According to Eqs S17 and S23 or S24, the initial branch populations in Eqs. S27 and S28 become:

$$[branch_1]_{F,0} = [branch_1]_{t_1} e^{-(k_{conv,F}+k_1)(t_{age}-t_1)} \quad \text{S30}$$

$$[branch_2]_{F,0} = \frac{k_c[branch_1]_{t_1}}{k_2-k_1-k_{conv,F}} e^{-(k_1+k_{conv,F})(t_{age}-t_1)} + \left([branch_2]_{t_1} - \frac{k_{conv,F}[branch_1]_{t_1}}{k_2-k_1-k_{conv,F}} \right) e^{-k_2(t_{age}-t_1)} \quad \text{S31}$$

$$k_2 \neq k_1 + k_{conv,F}$$

or

$$[branch_2]_{F,0} = \left(k_{conv,F}[branch_1]_{t_1}(t_{age}-t_1) + [branch_2]_{t_1} \right) e^{-k_2(t_{age}-t_1)}, \quad k_2 = k_1 + k_{conv,F} \quad \text{S32,}$$

where t_{age} is time of branching formation and subsequent aging.

The fractional amplitude of the slow $A_{s,F}$ (exponential) debranching phase under force is given by according to Eq. 29:

$$A_{s,F} = \frac{\frac{\left(k_{2,F} - k_{1,F}\right)[branch_1]_{F,0}}{k_{2,F} - k_{1,F} - k_{conv,F}}}{[branch_1]_{F,0} + [branch_2]_{F,0}} \qquad \text{S33}$$

which can be rewritten as:

$$= \frac{\frac{k_{2,F} - k_{1,F}}{k_{2,F} - k_{1,F} - k_{conv,F}}[branch_1]_{t_1} e^{-(k_{conv}+k_1)(t_{age}-t_1)}}{[branch_1]_{t_1} e^{-(k_{conv}+k_1)(t_{age}-t_1)} + \frac{k_{conv}[branch_1]_{t_1}}{k_2 - k_1 - k_{conv}} e^{-(k_1+k_{conv})(t_{age}-t_1)} + \left([branch_2]_{t_1} - \frac{k_{conv}[branch_1]_{t_1}}{k_2 - k_1 - k_{conv}}\right) e^{-k_2(t_{age}-t_1)}}$$

$$= \frac{\frac{k_{2,F} - k_{1,F}}{k_{2,F} - k_{1,F} - k_{conv,F}} e^{-(k_{conv}+k_1)(t_{age}-t_1)}}{\frac{k_2 - k_1}{k_2 - k_1 - k_{conv}} e^{-(k_1+k_{conv})(t_{age}-t_1)} + \left(\frac{[branch_2]_{t_1}}{[branch_1]_{t_1}} - \frac{k_{conv}}{k_2 - k_1 - k_{conv}}\right) e^{-k_2(t_{age}-t_1)}}$$

$$= \frac{\frac{\frac{k_{2,F} - k_{1,F}}{k_{2,F} - k_{1,F} - k_{conv,F}}}{\frac{[branch_2]_{t_1}}{[branch_1]_{t_1}} - \frac{k_{conv}}{k_2 - k_1 - k_{conv}}} e^{-(k_{conv}+k_1-k_2)(t_{age}-t_1)}}{1 + \frac{\frac{k_2 - k_1}{k_2 - k_1 - k_{conv}}}{\frac{[branch_2]_{t_1}}{[branch_1]_{t_1}} - \frac{k_{conv}}{k_2 - k_1 - k_{conv}}} e^{-(k_1+k_{conv}-k_2)(t_{age}-t_1)}} = \frac{be^{-(k_{conv}+k_1-k_2)(t_{age}-t_1)}}{1 + ae^{-(k_1+k_{conv}-k_2)(t_{age}-t_1)}}, \quad k_2 \neq k_1 + k_{conv} \qquad \text{S34}$$

when $k_2 \neq k_1 + k_{conv}$, and

$$= \frac{\frac{k_{2,F} - k_{1,F}}{k_{2,F} - k_{1,F} - k_{conv,F}}[branch_1]_{t_1} e^{-(k_{conv}+k_1)(t_{age}-t_1)}}{[branch_1]_{t_1} e^{-(k_{conv}+k_1)(t_{age}-t_1)} + \left(k_{conv}[branch_1]_{t_1}\left(t_{age} - t_1\right) + [branch_2]_{t_1}\right) e^{-k_2(t_{age}-t_1)}}$$

$$= \frac{\frac{k_{2,F} - k_{1,F}}{k_{2,F} - k_{1,F} - k_{conv,F}}}{\left(1 + \frac{[branch_2]_{t_1}}{[branch_1]_{t_1}} - k_{conv}t_1\right) + k_{conv}t_{age}} = \frac{1}{b' + a't_{age}}, \quad k_2 = k_1 + k_{conv} \qquad \text{S35}$$

when $k_2 = k_1 + k_{conv}$.

The fractional amplitude of the fast $A_{f,F}$ debranching phase under force is given by:

$$A_{f,F} = \frac{[branch_2]_{F,0} - \frac{k_{conv,F}[branch_1]_{F,0}}{k_{2,F} - k_{1,F} - k_{conv,F}}}{[branch_1]_{F,0} + [branch_2]_{F,0}} \qquad \text{S36}$$

which can be rewritten as

$$
\begin{aligned}
&\frac{k_{conv}[branch_1]_{t_1}}{k_2-k_1-k_{conv}}e^{-(k_1+k_{conv})(t_{age}-t_1)}+\left([branch_2]_{t_1}-\frac{k_{conv}[branch_1]_{t_1}}{k_2-k_1-k_{conv}}\right)e^{-k_2(t_{age}-t_1)}\\
&=\frac{-\dfrac{k_{conv,F}}{k_{2,F}-k_{1,F}-k_{conv,F}}[branch_1]_{t_1}e^{-(k_{conv}+k_1)(t_{age}-t_1)}}{\dfrac{k_2-k_1}{k_2-k_1-k_{conv}}[branch_1]_{t_1}e^{-(k_1+k_{conv})(t_{age}-t_1)}+\left([branch_2]_{t_1}-\dfrac{k_{conv}[branch_1]_{t_1}}{k_2-k_1-k_{conv}}\right)e^{-k_2(t_{age}-t_1)}}\\
&=\frac{1+\dfrac{\dfrac{k_{conv}}{k_2-k_1-k_{conv}}-\dfrac{k_{conv,F}}{k_{2,F}-k_{1,F}-k_{conv,F}}}{\dfrac{[branch_2]_{t_1}}{[branch_1]_{t_1}}-\dfrac{k_{conv}}{k_2-k_1-k_{conv}}}e^{-(k_{conv}+k_1-k_2)(t_{age}-t_1)}}{1+\dfrac{\dfrac{k_2-k_1}{k_2-k_1-k_{conv}}}{\dfrac{[branch_2]_{t_1}}{[branch_1]_{t_1}}-\dfrac{k_{conv}}{k_2-k_1-k_{conv}}}e^{-(k_1+k_{conv}-k_2)(t_{age}-t_1)}}\\
&=\frac{1+\dfrac{\dfrac{k_2-k_1}{k_2-k_1-k_{conv}}-\dfrac{k_{2,F}-k_{1,F}}{k_{2,F}-k_{1,F}-k_{conv,F}}}{\dfrac{[branch_2]_{t_1}}{[branch_1]_{t_1}}-\dfrac{k_{conv}}{k_2-k_1-k_{conv}}}e^{-(k_{conv}+k_1-k_2)(t_{age}-t_1)}}{1+\dfrac{\dfrac{k_2-k_1}{k_2-k_1-k_{conv}}}{\dfrac{[branch_2]_{t_1}}{[branch_1]_{t_1}}-\dfrac{k_{conv}}{k_2-k_1-k_{conv}}}e^{-(k_1+k_{conv}-k_2)(t_{age}-t_1)}}\\
&=\frac{1+(a-b)e^{-(k_{conv}+k_1-k_2)(t_{age}-t_1)}}{1+ae^{-(k_1+k_{conv}-k_2)(t_{age}-t_1)}}=1-A_{s,F},\quad k_2\neq k_1+k_{conv}
\end{aligned}
\tag{S37}
$$

when $k_2 \neq k_1 + k_{conv}$, and

$$
\begin{aligned}
&\frac{\left(k_{conv}[branch_1]_{t_1}(t_{age}-t_1)+[branch_2]_{t_1}\right)e^{-k_2(t_{age}-t_1)}-\dfrac{k_{conv,F}}{k_{2,F}-k_{1,F}-k_{conv,F}}[branch_1]_{t_1}e^{-(k_{conv}+k_1)(t_{age}-t_1)}}{[branch_1]_{t_1}e^{-(k_{conv}+k_1)(t_{age}-t_1)}+\left(k_{conv}[branch_1]_{t_1}(t_{age}-t_1)+[branch_2]_{t_1}\right)e^{-k_2(t_{age}-t_1)}}\\
&=\frac{\dfrac{[branch_2]_{t_1}}{[branch_1]_{t_1}}-\dfrac{k_{conv,F}}{k_{2,F}-k_{1,F}-k_{conv,F}}-k_{conv}t_1+k_{conv}t_{age}}{1+\dfrac{[branch_2]_{t_1}}{[branch_1]_{t_1}}-k_{conv}t_1+k_{conv}t_{age}}\\
&=\frac{b'-1+a't_{age}}{b'+a't_{age}}=1-\frac{1}{b'+a't_{age}}=1-A_{s,F},\quad k_2=k_1+k_{conv}
\end{aligned}
\tag{S38}
$$

when $k_2 = k_1 + k_{conv}$. Eqs. S35 and S38 indicate that when $k_2 = k_1 + k_{conv}$, the fractional fast and slow amplitudes depend hyperbolically on the age time (t_{age}).

In the above equations, the constants a, a', b, and b' are defined by:

$$a = \frac{\dfrac{k_2 - k_1}{k_2 - k_1 - k_{conv}}}{\dfrac{[branch_2]_{t_1}}{[branch_1]_{t_1}} - \dfrac{k_{conv}}{k_2 - k_1 - k_{conv}}}, \quad b = \frac{\dfrac{k_{2,F} - k_{1,F}}{k_{2,F} - k_{1,F} - k_{conv,F}}}{\dfrac{[branch_2]_{t_1}}{[branch_1]_{t_1}} - \dfrac{k_{conv}}{k_2 - k_1 - k_{conv}}} \qquad \text{S39}$$

$$a' = \frac{k_{conv}}{\dfrac{k_{2,F} - k_{1,F}}{k_{2,F} - k_{1,F} - k_{conv,F}}}, \quad b' = \frac{1 + \dfrac{[branch_2]_{t_1}}{[branch_1]_{t_1}} - k_{conv} t_1}{\dfrac{k_{2,F} - k_{1,F}}{k_{2,F} - k_{1,F} - k_{conv,F}}} \qquad \text{S40.}$$

4) *Determination of the branch formation, conversion, and debranching rate constants in the absence of force*. Global fitting of the aging time-dependent time courses of debranching under force to a double exponential equation (Fig. 2B) yielded slow ($k_{s,F}$) and fast ($k_{f,F}$) phase observed rate constants, expressed as slow and fast lifetimes ($\tau = 1/k_{obs}$), values of $\tau_{s,F} = 3.08 \pm 0.05$ and $\tau_{f,F} = 0.15 \pm 0.01$ min. According to Eq. S29, the corresponding rate constants are given by:

$$k_{s,F} = k_{1,F} + k_{conv,F} = \frac{1}{\tau_s} = 0.32 \pm 0.005 \text{ min}^{-1}$$
$$k_{f,F} = k_{2,F} = \frac{1}{\tau_f} = 6.67 \pm 0.44 \text{ min}^{-1} \qquad \text{S41.}$$

The amplitudes from the double exponential fit reflect the distribution between the two Arp2/3 branch states ($branch_1$ and $branch_2$) populated during aging in the absence of force, as described by Eqs. S34 and S37.

Global analysis of the aging time-dependence of the slow and fast phase amplitudes using Eqs. S34 and S37 (Eq. 2 in main text), and the branch formation time $t_1 = 2.6$ min yielded the following parameters in the absence of force (Fig. 4C):

$$k_1 + k_{conv} - k_2 = 0.14 \pm 0.03 \text{ min}^{-1}$$
$$a = 0.01 \pm 0.12 \qquad \text{S42.}$$
$$b = 2.0 \pm 0.4$$

When the aging time equals the branch formation time, i.e., $t_{age} = t_1$, the fractional amplitudes for debranching under force are $A_{s,F} \sim 1$ and $A_{f,F} \sim 0$ (Fig. 4C). According to Eqs. S33 and S36 , the fractional amplitudes of the slow and fast phases at $t_{age} = t_1$ are:

$$A_{s,F}\left(t_{age} = t_1\right) = \frac{\dfrac{\left(k_{2,F} - k_{1,F}\right)[branch_1]_{t_1}}{k_{2,F} - k_{1,F} - k_{conv,F}}}{[branch_1]_{t_1} + [branch_2]_{t_1}} \sim 1 \qquad \text{S43}$$

$$A_{f,F}\left(t_{age} = t_1\right) = \frac{[branch_2]_{t_1} - \dfrac{k_{conv,F}}{k_{2,F} - k_{1,F} - k_{conv,F}}[branch_1]_{t_1}}{[branch_1]_{t_1} + [branch_2]_{t_1}} \sim 0 \qquad \text{S44.}$$

The ratio of the two branch states formed during the initial branch formation time is given by:

$$\frac{[branch_2]_{t_1}}{[branch_1]_{t_1}} \sim \frac{k_{conv,F}}{k_{2,F} - k_{1,F} - k_{conv,F}} < \frac{k_{conv,F} + k_{1,F}}{k_{2,F} - k_{1,F} - k_{conv,F}} \sim 0.05 \qquad \text{S45,}$$

as estimated from the experimentally determined rate constants under force (Eq. S41). Therefore, $[branch_2] \sim 0$ upon conclusion of branch formation time t_1. That is, little or no conversation occurs within the first 2.6 min of

aging and most (>95%) of branches remain in the $branch_1$ state. Given this value and Eq. S39 with the experimental value $a = 0.01$ (S42),

$$a = \frac{\dfrac{k_2 - k_1}{k_2 - k_1 - k_{conv}}}{\dfrac{[branch_2]_{t_1}}{[branch_1]_{t_1}} - \dfrac{k_{conv}}{k_2 - k_1 - k_{conv}}} \sim -\frac{k_2 - k_1}{k_{conv}} = 0.01 \qquad \text{S46.}$$

According to Eq. S46 and the rate constant in Eq. S42, the calculated value of k_{conv} is:

$$k_{conv} = \frac{0.14}{1.01} \sim 0.14 \pm 0.03 \text{ min}^{-1} \qquad \text{S47.}$$

The standard deviation for k_{conv} calculated according to error propagation:

$$\delta k_{conv} = \sqrt{\frac{\delta r^2}{(1+a)^2} + \frac{r^2 \delta a^2}{(1+a)^4}} \qquad \text{S48,}$$

where r is ($k_1 + k_{conv} - k_2$) in the absence of force, and the standard errors $\delta r = 0.03$ and $\delta a = 0.12$ (Eq. S42).

Since the conversion rate constant $k_{conv} = 0.14$ min^{-1} (lifetime for conversion ~ 7 min), conversion from state 1 to state 2 is nearly complete within 30 min age time. This is why time courses of debranching after 30 min aging follow single exponential.

Given this value of k_{conv} value and Eq. S42, yields $k_1 - k_2 \sim 0.0014$ min^{-1} ~ 0 min^{-1}, indicating that $k_1 \sim k_2$, with k_1 slightly larger than k_2. The lifetime of debranching in the absence of force estimated from the force-dependence of debranching after 30 min aging (Fig. 2D) is 106 (± 8) min ($k_{obs} = 0.01 \pm 0.007$ min^{-1}). Since conversion from state 1 to state 2 is completed within 30 min, debranching after a 30 min age time occurs exclusively from state 2. Accordingly, this k_{obs} reflects debranching from state 2 ($k_2 = 0.01 \pm 0.007$ min^{-1}; Table 1). The rate constant for debranching from state 1 in the absence of force is estimated to be $k_1 \sim 0.011$ min^{-1}. Since $k_1 \sim k_2$, the fast exponential term amplitude in the observed debranching time course under no force (Eq. S25) is ~ 0 and the time course reduce to a single exponential decay.

Eq. S4 above represents the rate constant for branch formation during the initial branch formation age time t_1. Since k_1 and k_2 are small compared to both k_{conv} and $k_{form}[Arp]$, the two observed rate constants in Eq. S4 can be approximated as:

$$\lambda_{form,+} = k_{form}[Arp], \quad \lambda_{form,-} = k_{conv} \qquad \text{S49.}$$

During the branch formation time t_1 of 2.6 min, $[branch_2] \sim 0$ (Eq. S14), yields

$$\frac{k_{conv}}{-\lambda_{form,+} + \lambda_{form,-}} \left(-\lambda_{form,-} e^{-\lambda_{form,+} t_1} + \lambda_{form,+} e^{-\lambda_{form,-} t_1} \right) + k_{conv} \sim 0 \qquad \text{S50,}$$

which can be rearranged to:

$$\frac{1 - e^{-\lambda_{form,-} t_1}}{\lambda_{form,-}} = \frac{1 - e^{-\lambda_{form,+} t_1}}{\lambda_{form,+}} \qquad \text{S51.}$$

Assuming $\lambda_{form,+}\, t_1 << 1$ or $t_1 << 1/\lambda_{form,+}$, a Taylor expansion of the exponential function in S51 with $\lambda_{form,+}\, t_1$ to 2nd order yields:

$$= \frac{1-\left(1-\lambda_{form,+}t_1+\frac{1}{2}\lambda_{form,+}{}^2t_1{}^2+O\left(\lambda_{form,+}{}^3t_1{}^3\right)\right)}{\lambda_{form,+}}$$

$$= t_1-\frac{1}{2}\lambda_{form,+}t_1{}^2+O\left(\lambda_{form,+}{}^2t_1{}^3\right) \quad \text{S52.}$$

Given t_1 = 2.6 min and $\lambda_{form,-} \sim k_{conv}$ values (Eq. S49), solving Eq. S51-52 yields

$$\lambda_{form,+} = k_{form}[Arp] = 2\left(\frac{1}{t_1}-\frac{1-e^{-\lambda_{form,-}t_1}}{t_1{}^2\lambda_{form,-}}\right) = 2\left(\frac{1}{t_1}-\frac{1-e^{-k_{conv}t_1}}{t_1{}^2k_{conv}}\right) = 0.12 \text{ min}^{-1} \quad \text{S53.}$$

Debranching experiments were carried out with 0.1 μM Arp2/3. Therefore, the of 2nd order association rate constant for branch formation, $k_{form} = \lambda_{form,+}/[Arp]$ = 1.2 μM^{-1} min^{-1} = 0.02 μM^{-1} sec^{-1}. This rate constant reflects a composite of Arp2/3 binding and subsequent branch formation.

Using the two observed rate constants (Eqs. S47, S49 and S53) for branch formation in Eq. S14, time course of branch formation in the absence of force during time t_1 follow single exponentials and can be constructed from:

$$[branch] = [branch_1]+[branch_2]$$

$$= q\left(-\frac{\lambda_{form,-}\left(k_2-\lambda_{form,+}\right)}{-\lambda_{form,+}+\lambda_{form,-}}e^{-\lambda_{from,+}t}+\frac{\lambda_{form,+}\left(k_2-\lambda_{form,-}\right)}{-\lambda_{form,+}+\lambda_{form,-}}e^{-\lambda_{form,-}t}+k_2\right.$$

$$\left.\frac{k_{conv}}{-\lambda_{form,+}+\lambda_{form,-}}\left(-\lambda_{form,-}e^{-\lambda_{form,+}t}+\lambda_{form,+}e^{-\lambda_{form,-}t}\right)+k_{conv}\right)$$

$$= qk_{conv}\left(1-e^{-\lambda_{from,+}t}\right) \quad \text{S54,}$$

where $k_2 \sim 0$ and $\lambda_{form,-} \sim k_{conv}$.

Part 3. A model for the distribution of branches at the leading edge of cells based on the dependence of the rates of branch dissociation on age and applied force.

The model

We present a minimal kinetic model to assess how the effects of aging, force and GMF on dissociation of branches formed by Arp2/3 complex might explain density of actin filament branches at the leading edge of a motile cell or equivalent situations as a *Listeria* comet tail; Fig. S9). The model assumes (a) that branches form from ATP-Arp2/3 complex only at the leading edge (8), where nucleation promoting factors activate Arp2/3 complex (b) hydrolysis of ATP rapidly converts to Arp2/3 complex in branches to ADP-P_i followed by slow phosphate dissociation, (c) force applied at the leading edge membrane is uniformly distributed throughout the filament network, and (d) the whole network migrates by retrograde flow perpendicular to the cell membrane at the leading edge (i.e. towards the cell interior; Fig. S9) at a constant velocity (v) that is *relative* to and independent of leading edge movement. To an observer, the leading edge is on a *y*-*z* plane at $x = 0$, while the network migrates in the *x*-axis direction by retrograde flow towards the cell interior (Fig. S9). The branches in any efficiently small volume ΔV (Fig. S9, black cube) within the network dissociate as the volume move away from the initial position at the leading edge.

Branches formed by Arp2/3 complex dissociate by two pathways (Scheme S2 above repeated here for convenience):

$$\begin{array}{ccc} branch_1 & \xrightarrow{k_{conv,F}} & branch_2 \\ \downarrow k_{1,F} & & \downarrow k_{2,F} \\ & debranched & \end{array} \qquad \text{Scheme S2,}$$

where $branch_1$ has ADP-P_i bound to Arp2/3 complex, $branch_2$ has ADP bound to Arp2/3 complex, $k_{1,F}$ is the dissociation rate constant for branches with ADP-P_i-Arp2/3 complex, $k_{2,F}$ is the dissociation rate constant for branches with ADP-Arp2/3 complex, and $k_{conv,F}$ is the rate constant for conversion of Arp2/3 complex from the ADP-P_i to ADP state. Force can influence all three rate constants. In this model the distribution of branches is uniform along the *y*- and *z*- directions (i.e. uniform in any *y*-*z* plane along the *x*-axis), but varies along *x*-axis due to branch dissociation. In the absence of force $k_{conv} >> k_1$, so debranching occurs predominately from the branch 2 state and time courses follow single exponentials (Fig. 4B). In the presence of force debranching occurs from both the branch 1 and 2 states.

Branch density distribution

The parallel pathway depicted in Scheme S2 predicts debranching time courses that follow a double exponential decay. Under initial conditions, $t = 0$ and the leading edge, where $[branch_1] = [branch_1]_0$ and $[branch_2] = 0$, the exact solution of Scheme S2 (i.e. the time dependence of the total combined branches in the two states) can be obtained following the same procedure above (from Eq. S15 to S26) as follows:

$$\begin{aligned} &[branch] = [branch_1] + [branch_2] \\ &= [branch_1]_0 e^{-\left(k_{1,F}+k_{conv,F}\right)t} + \frac{k_{conv,F}[branch_1]_0}{k_{2,F}-k_{1,F}-k_{conv,F}}\left(e^{-\left(k_{1,F}+k_{conv,F}\right)t} - e^{-k_{2,F}t}\right) \\ &= \frac{[branch_1]_0}{k_{2,F}-k_{1,F}-k_{conv,F}}\left(\left(k_{2,F}-k_{1,F}\right)e^{-\left(k_{1,F}+k_{conv,F}\right)t} - k_{conv,F}e^{-k_{2,F}t}\right), \quad k_{2,F} \neq k_{1,F}+k_{conv,F} \end{aligned}$$

or

$$\begin{aligned}[branch] &= [branch_1] + [branch_2] \\ &= [branch_1]_0 e^{-\left(k_{1,F}+k_{conv,F}\right)t} + k_{conv,F}[branch_1]_0 te^{-k_{2,F}t} \\ &= [branch_1]_0 \left(1 + k_{conv,F}t\right)e^{-k_{2,F}t}, \quad k_{2,F} = k_{1,F} + k_{conv,F}\end{aligned} \tag{S56}$$

Note that the initial conditions in the derivation Eqs S15-S26 and the solution represented by Eqs. S25 and S26 are slightly different. If $k_{1,F} \sim k_{2,F}$, the first exponential term in Eq. 55 disappears and the combined total branches of two states follow a single exponential decay (see below).

Since the small sample volume (ΔV) travels away from membrane with a constant relative velocity ν in the x direction, the distance from the membrane at time t is $x = \nu t$. Substituting $t = x/\nu$ into Eqs. S55 and S56, yields the spatial distribution of branch concentration in the x-axis direction:

$$[branch] = \frac{[branch_1]_0}{k_{2,F} - k_{1,F} - k_{conv,F}}\left(\left(k_{2,F} - k_{1,F}\right)e^{-\frac{\left(k_{1,F}+k_{conv,F}\right)x}{\nu}} - k_{conv,F}e^{-\frac{k_{2,F}x}{\nu}}\right), \tag{S57}$$

$$k_{2,F} \neq k_{1,F} + k_{conv,F}$$

or

$$[branch] = [branch_1]_0\left(1 + \frac{k_{conv,F}x}{\nu}\right)e^{-\frac{k_{2,F}x}{\nu}}, \quad k_{2,F} = k_{1,F} + k_{conv,F} \tag{S58}$$

In general, when $k_{2,F} \neq k_{1,F} + k_{conv,F}$, the spatial distribution of the branch concentration follows a double exponential decay towards the cell interior with a total amplitude given by the initial branch concentration at the membrane ($[branch_1]_0$). The overall "decay length" of the double exponential decay is discussed below. In a rare, special case, when, when $k_{2,F} = k_{1,F} + k_{conv,F}$, the branch concentration spatial distribution follows a single exponential decay (see also (9-12)) toward the cell interior with additional non-exponential terms. Since this is a rare and special case, we focus our discussion on the general case when $k_{2,F} \neq k_{1,F} + k_{conv,F}$.

Average branched actin network boundary opposite to the leading edge membrane

In a small time interval $\Delta t = (t - t+\Delta t)$, the number of branches (ΔN) that have dissociated from the small sampled volume ΔV is given by

$$\Delta N = \left([branch]_{t+\Delta t} - [branch]_t\right)\Delta V = \frac{d[branch]_t}{dt}\Delta V \Delta t \tag{S59,}$$

and those dissociated branches during Δt have lifetime $\tau = t$. Therefore, the average lifetime ($\bar{\tau}$) of branches dissociated at different times is given by

$$\bar{\tau} = \frac{\sum_n t_n \Delta N\left(t_n\right)}{\sum_n \Delta N\left(t_n\right)} = \frac{\int_0^\infty t\frac{d[branch]_t}{dt}\Delta V dt}{\int_0^\infty \frac{d[branch]_t}{dt}\Delta V dt}$$

$$= \frac{t[branch]\big|_0^\infty - \int_0^\infty [branch]_t\, dt}{[branch]\big|_{t=\infty} - [branch]\big|_{t=0}} = \frac{\int_0^\infty [branch]_t\, dt}{[branch_1]_0} \qquad \text{S60}$$

According to the time-dependent branch concentration expression in Eqs. S55 or S56, the boundary values, $[branch]|_{t=\infty} = t[branch]|_{t=\infty} = t[branch]|_{t=\infty} = 0$ and $[branch]|_{t=0} = [branch_1]_0$ can be evaluated easily. When $k_{2,F} \neq k_{1.F} + k_{conv,F}$, according to Eq. S55, the average lifetime ($\bar{\tau}$) in Eq. S60 becomes

$$= \int_0^\infty \frac{\left(k_{2,F} - k_{1,F}\right) e^{-\left(k_{1,F}+k_{conv,F}\right)t} - k_{conv,F} e^{-k_{2,F}t}}{k_{2,F} - k_{1,F} - k_{conv,F}}\, dt$$

$$= \left. \frac{-\frac{k_{2,F} - k_{1,F}}{k_{1,F} + k_{conv,F}} e^{-\left(k_{1,F}+k_{conv,F}\right)t} + \frac{k_{conv,F}}{k_{2,F}} e^{-k_{2,F}t}}{k_{2,F} - k_{1,F} - k_{conv,F}} \right|_0^\infty$$

$$= \frac{\frac{k_{2,F} - k_{1,F}}{k_{1,F} + k_{conv,F}} - \frac{k_{conv,F}}{k_{2,F}}}{k_{2,F} - k_{1,F} - k_{conv,F}}, \quad k_{2,F} \neq k_{1,F} + k_{conv,F} \qquad \text{S61.}$$

When $k_{2,F} = k_{1.F} + k_{conv,F}$, according to Eq. S56, the average lifetime ($\bar{\tau}$) becomes

$$= \int_0^\infty \left(1 + k_{conv,F} t\right) e^{-k_{2,F}t} dt = -\frac{1}{k_{2,F}} \left(\left(1 + k_{conv,F} t\right) e^{-k_{2,F}t} \Big|_0^\infty - \int_0^\infty k_{conv,F} e^{-k_{2,F}t} dt \right)$$

$$= \frac{1}{k_{2,F}} \left(1 + \frac{k_{conv,F}}{k_{2,F}} \right), \quad k_{2,F} = k_{1,F} + k_{conv,F} \qquad \text{S62.}$$

All branches in an actin network dissociate at average time as expressed in Eq. S61 or S62. At the average lifetime ($\bar{\tau}$), the average length of the branch distribution ($\bar{d}$; i.e. the distance, or "decay length" at which all branches dissociate) away from membrane in the *x*-direction is given by:

$$\bar{d} = v\bar{t} = \begin{cases} v \dfrac{\frac{k_{2,F} - k_{1,F}}{k_{1,F} + k_{conv,F}} - \frac{k_{conv,F}}{k_{2,F}}}{k_{2,F} - k_{1,F} - k_{conv,F}}, & k_{2,F} \neq k_{1,F} + k_{conv,F} \\ v \dfrac{1}{k_{2,F}} \left(1 + \dfrac{k_{conv,F}}{k_{2,F}} \right), & k_{2,F} = k_{1,F} + k_{conv,F} \end{cases} \qquad \text{S63.}$$

For branches whose time after formation is shorter than the average branch lifetime, their distance away from membrane is shorter than the "decay length" and the population does not dissociate completely. Therefore, this

average distance in *x*-direction ($\bar{d}$; Eq. S63) is also the average length, of the branched actin network from the cell membrane at the cell leading edge in the *x*-direction.

Effects of force on the branched actin network architecture

The results presented in this study indicate that in the absence of force (F = 0), $k_{2,F} = k_{1.F} \sim 0.01$ min^{-1}. Eq. S57 predicts that the branched actin network distribution along *x*-axis follows a single exponential according to:

$$[branch] = [branch_1]_{0,F=0} e^{-\frac{k_{2,F}x}{\nu}} = [branch_1]_{0,F=0} e^{-0.01\frac{x}{\nu}} \quad \text{S64}$$

and according to Eq. S63, the network length in the *x*-direction is given by:

$$\bar{d} = \nu \frac{\frac{k_{2,F} - k_{1,F}}{k_{1,F} + k_{conv,F}} - \frac{k_{conv,F}}{k_{2,F}}}{k_{2,F} - k_{1,F} - k_{conv,F}} = \frac{\nu}{k_{2,F}} = 100\nu \quad \text{S65.}$$

Under 500 μL min^{-1} flow rate, the average force F is ~1 pN for 1.5 μm branch length, and $k_{1.F}+k_{conv,F} \sim 0.32$ and $k_{2,F} \sim 6.67$ min^{-1} (Eq. S41). Under these conditions, the branch distribution (Eq. S57) is given by:

$$\begin{aligned}
[branch] &= \frac{[branch_1]_{0,F}}{k_{2,F} - k_{1,F} - k_{conv,F}} \left(\left(k_{2,F} - k_{1,F}\right) e^{-\frac{\left(k_{1,F} + k_{conv,F}\right)x}{\nu}} - k_{conv,F} e^{-\frac{k_{2,F}x}{\nu}} \right) \\
&= \frac{[branch_1]_{0,F}}{6.67 - 0.32} \left(\left(6.67 - k_{1,F}\right) e^{-\frac{0.32x}{\nu}} - k_{conv,F} e^{-\frac{6.67x}{\nu}} \right) \\
&\sim \frac{[branch_1]_{0,F}}{6.67} \left(6.67 e^{-\frac{0.32x}{\nu}} - k_{conv,F} e^{-\frac{6.67x}{\nu}} \right) \\
&= [branch_1]_{0,F} e^{-\frac{6.67x}{\nu}} \left(e^{\frac{6.67-0.32}{\nu}x} - \frac{k_{conv,F}}{6.67} \right) \\
&\sim [branch_1]_{0,F} \left(e^{-\frac{0.32x}{\nu}} - 0 \right) = [branch_1]_{0,F} e^{-\frac{0.32x}{\nu}}
\end{aligned} \quad \text{S66.}$$

Since $k_{1.F}+k_{conv,F} \sim 0.32$ min^{-1}, the maximum value of $k_{1.F}$ and $k_{conv,F}$ is 0.32 << $k_{2,F} \sim 6.67$ min^{-1}. Also, $e^{\frac{6.67-0.32}{\nu}x} = e^{\frac{6.35}{\nu}x} > 1 >> \frac{k_{conv}}{6.67}$. Under those approximations, the branch density distribution is approximately a single exponential as well and its average length in *x*-direction is given by:

$$\bar{d} = \nu \frac{\frac{k_{2,F} - k_{1,F}}{k_{1,F} + k_{conv,F}} - \frac{k_{conv,F}}{k_{2,F}}}{k_{2,F} - k_{1,F} - k_{conv,F}} \sim \nu \frac{\frac{6.67 - 0}{0.32} - 0}{6.67 - 0.32} \sim \frac{\nu}{0.32} \sim 3\nu \quad \text{S67}$$

Comparison of the branch distribution and average network length with and without pico-newton force (Eqs. S64 vs. S66 and S65 vs. S67), indicates that the branch distribution decay 32 times faster and average length of the branched network in the *x*-direction is 32-fold shorter, or narrower under force.

This comparison is one example how force would modify branched actin network architecture, and assumes similar network velocity v with and without force. The value of v can change with force, and the branched actin network density decay rate constant and network length would change according to Eqs. S57 or S58, and S63. In addition, force could potentially affect the branch formation at the membrane, which would also cause the initial branch concentration $[branch_1]_0$ at the membrane region to change. Note, however, that changes in Arp2/3 complex activation affect only the amplitude of the network density decay, not the decay constant or average network length along the *x*-direction. The effect of force on preferentially debranching of "old" ADP-Arp 2/3 complex branches over young ADP-P_i Arp2/3 complexes shortens the decay length (e.g. narrows the network).

Eqs. S66 and S67 hold under any force, provided that "old" branches with ADP Arp2/3 complex dissociate much faster (given by $k_{2,F}$) than "young" branches with ADP-P_i-Arp2/3 complex (given by $k_{1,F}$) combined with conversion (given by $k_{conv,F}$; i.e. $k_{2,F} >> k_{1,F} + k_{conv,F}$). When these conditions are satisfied, the branched actin network distribution follows a single exponential with a decay constant proportional to $k_{1.F}+k_{conv,F}$ (Eq. S66) and the network average length is inversely proportional to $k_{1.F}+k_{conv,F}$ (Eq. S67).

We now consider only cases in which this condition applies. Assuming the debranching and conversion rate constants are force sensitive and related through Bell's equation (Eq. 1 in main text), substituting Bell's equation to Eqs. S66 and S67 yields the force dependence of branched network distribution and average network length:

$$[branch] \sim [branch_1]_{0,F} e^{-\frac{\left(k_{1,F}+k_{conv}\right)x}{v}} = [branch_1]_{0,F} e^{-\frac{\left(k_{1,F=0}e^{-Fd_1/k_BT}+k_{conv,F=0}e^{-Fd_{conv}/k_BT}\right)x}{v}} \quad \text{S68}$$

$$\bar{d} \sim \frac{v}{k_{1,F}+k_{conv}} = \frac{v}{k_{1,F=0}e^{-Fd_1/k_BT}+k_{conv,F=0}e^{-Fd_{conv}/k_BT}} \quad \text{S69.}$$

The average branch density across the actin filament network for a network distribution following a single exponential decay can be calculated by the following integration.

$$\overline{[branch]}_F = \frac{\int_0^\infty \left([branch]\right)^2 dx}{\int_0^\infty [branch]dx} = \frac{\int_0^\infty \left([branch_1]_{0,F} e^{-\frac{\left(k_{1,F}+k_{conv,F}\right)x}{v}} \right)^2 dx}{\int_0^\infty [branch_1]_{0,F} e^{-\frac{\left(k_{1,F}+k_{conv,F}\right)x}{v}} dx} \quad \text{S70,}$$

$$= \frac{[branch_1]_{0,F}}{2} \frac{\Gamma(1)}{\Gamma(1)} = \frac{[branch_1]_{0,F}}{2}$$

where $\Gamma(x) = \int_0^\infty t^{x-1} e^{-t} dt$ is gamma function and Γ(1) = 1. Therefore, the average branch density is half of the initial density of branches formed at membrane (amplitude) and is determined only by the amplitude independent of the network density decay constant.

This minimal model does not consider debranching by other factors and regulatory proteins such as GMF and cofilin. If the contribution of these debranching proteins is accounted for, the branched actin network would decay even faster and the network length would be even narrower. Note that the preferential dissociation of "old" branches by GMF will introduce effects to those of force.

Fig. S10 illustrates actin network branch density distribution along the *x*-direction in the presence or absence of force with different levels of branch formation at the leading edge ($[branch_1]_{0,F}$). When the total number of branches in the network is conserved and Arp2/3 complexes released from branches are rapidly recycled at the leading edge, the new branch formation at the leading edge ($[branch_1]_{0,F}$) increases in proportion to the enhanced debranching under force.

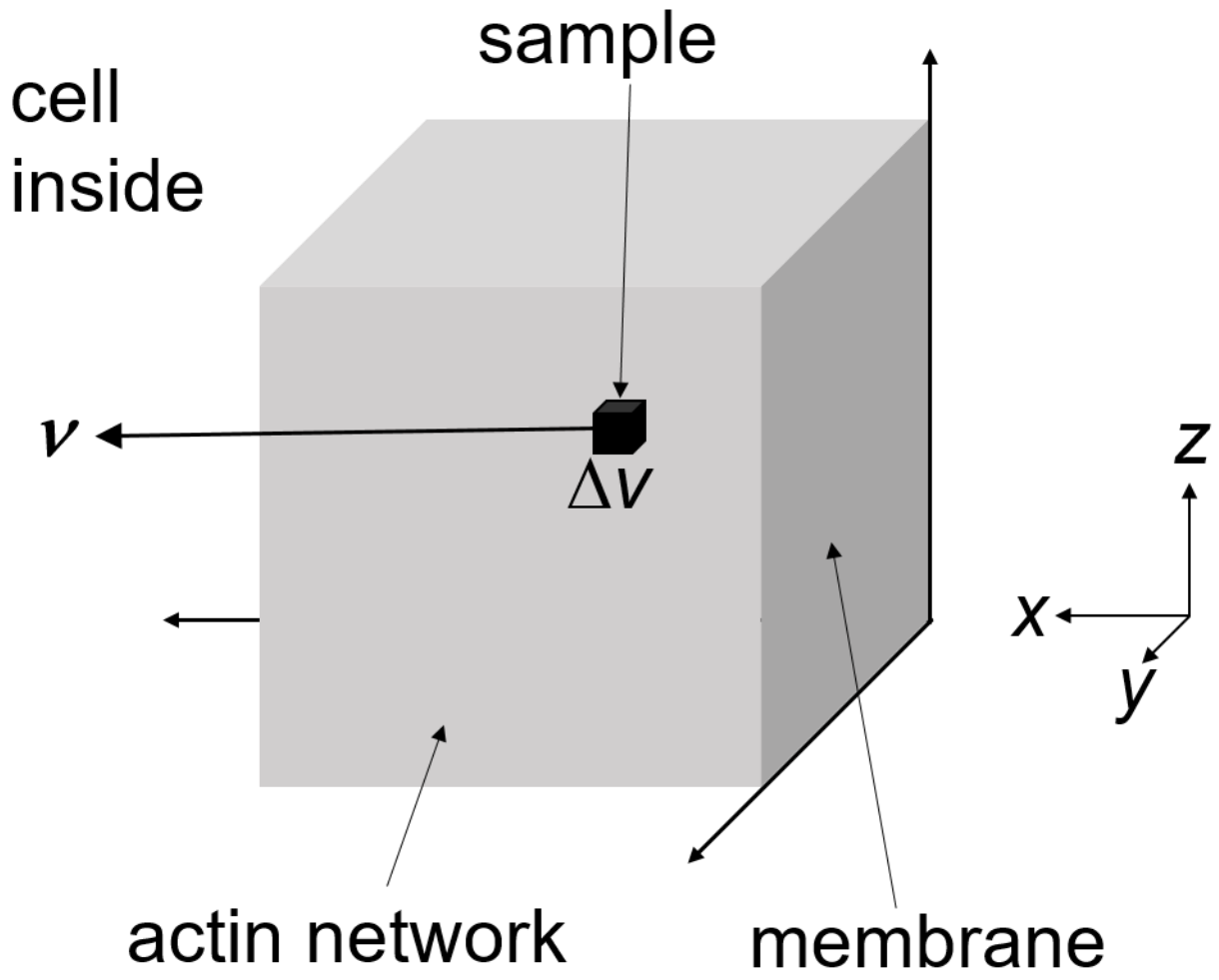

Figure S9: Illustration of the actin branched network formation and internal migration near plasma membrane at the leading edge of a cell. The membrane is on the *y*-*z* plane at $x = 0$. The branched actin network internally migrates by retrograde flow at a constant relative velocity v (x direction) towards the cell interior (grey). We note that the depicted boundaries of the cube do not represent actual network boundaries. The distance between top and bottom edges in *z*-direction is very narrow for lamellipodia and the network is essentially a flat sheet in the *x*-*y* plane.

.

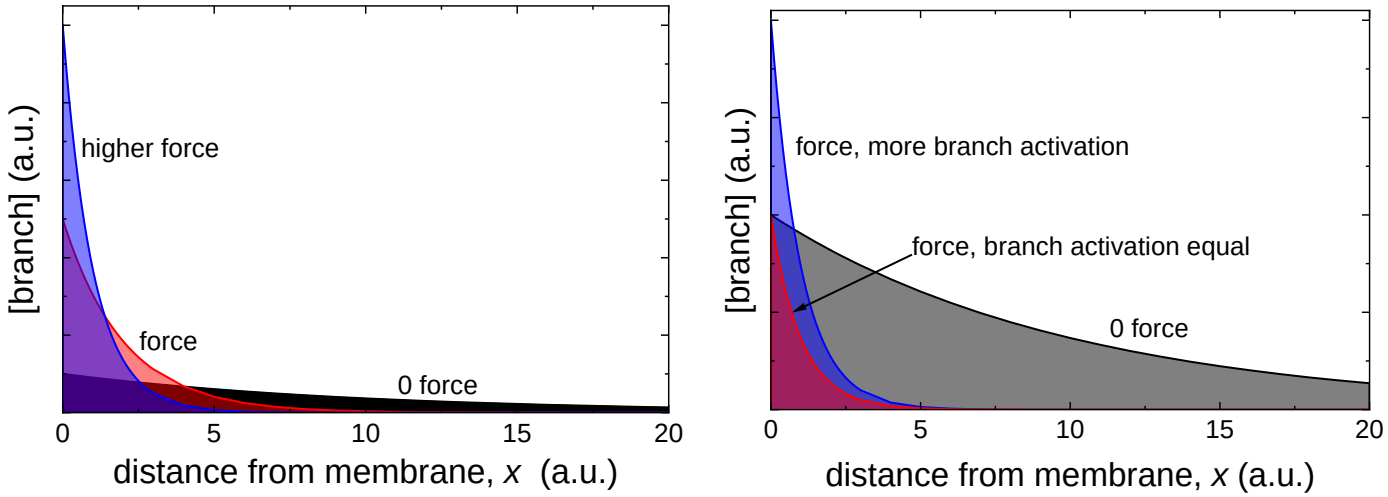

Figure S10. Calculation using Eq. S66 of the distributions of actin filament branches in the leading edge networks in the presence and absence of force. Left: Comparison of the distribution of branches in the network under no force (black), an arbitrary force ("force"; red) and a second arbitrary, but higher force ("higher force"; blue), under conditions when the total number of branches in the network is constant. The decay constants were chosen to be 5-fold larger than in the absence of force for "certain force" and 10-fold higher for the "higher force," both less than the 32-fold change in the decay constant caused by low pN forces in our experiments (Eqs. S64 and S66). Right: Comparison of the distribution of branches in the network with (red and blue) and without (grey) force when branch formation at the leading edge is higher under force (i.e. total number of branches is not necessarily conserved). The decay constant under force was set to be 10-fold larger than in the absence of force. Increasing branch formation 2-fold under force (blue) increases the average network branch density across the network 2-fold (Eq. S70), but decreases, in this special case, the total number of branches in the network (total area under curve) compared to no force (grey). On the other hand, when branch formation at the leading edge is not activated by force (red), the average branch density across the network is the same as in the absence of force (Eq. S70), but the total number of branches decreases.

Part 4. DNA sequence of GMF

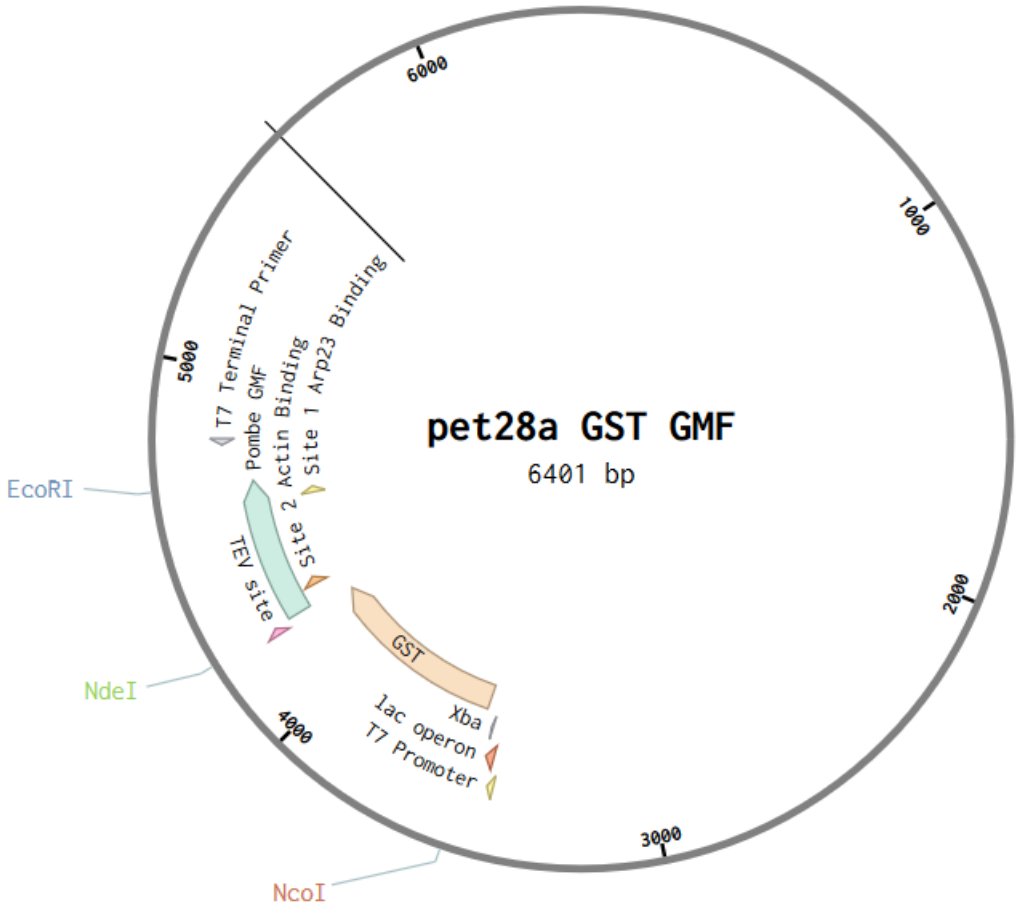

GMF (Glia Maturation Factor) Pombe DNA Sequence:
ATGTCATCAGAGGCTCGTATGTTCACCATTTCGGATACCACGATGAAAGAAATTGATCGATTTCGT
TTGCGGTTGAAGAAATCAGTTATGTATGCTTTCATTCTCAAGGTTGATAAAGCTACTAAGGAGATT
GTTCCCGATGGAGAAATCATGGATTTACAGAGTATTGAAGAGGTCGCAGATGAACTCTCGGAAAC
AAATCCTAGATTTATCCTTGTTTCCTATCCTACCAAAACCACAGATGGTCGACTTAGTACTCCATTG
TTTATGATATACTGGAGACCAAGTGCTACCCCAAATGACTTATCTATGATTTATGCTTCTGCTAAA
GTCTGGTTTCAAGATGTGTCGCAGGTGCACAAAGTATTTGAAGCTAGAGATTCTGAAGATATTACT
AGTGAAGCAGTTGATGAGTTTTTGCATTAA

Pet28A-GST-GMF DNA Sequence
TTGCAAACAAAAAAACCACCGCTACCAGCGGTGGTTTGTTTGCCGGATCAAGAGCTACCAACTCTT
TTTCCGAAGGTAACTGGCTTCAGCAGAGCGCAGATACCAAATACTGTCCTTCTAGTGTAGCCGTAG
TTAGGCCACCACTTCAAGAACTCTGTAGCACCGCCTACATACCTCGCTCTGCTAATCCTGTTACCA
GTGGCTGCTGCCAGTGGCGATAAGTCGTGTCTTACCGGGTTGGACTCAAGACGATAGTTACCGGAT
AAGGCGCAGCGGTCGGGCTGAACGGGGGGTTCGTGCACACAGCCCAGCTTGGAGCGAACGACCT
ACACCGAACTGAGATACCTACAGCGTGAGCTATGAGAAAGCGCCACGCTTCCCGAAGGGAGAAA
GGCGGACAGGTATCCGGTAAGCGGCAGGGTCGGAACAGGAGAGCGCACGAGGGAGCTTCCAGGG

GGAAACGCCTGGTATCTTTATAGTCCTGTCGGGTTTCGCCACCTCTGACTTGAGCGTCGATTTTTGT
GATGCTCGTCAGGGGGGCGGAGCCTATGGAAAAACGCCAGCAACGCGGCCTTTTTACGGTTCCTG
GCCTTTTGCTGGCCTTTTGCTCACATGTTCTTTCCTGCGTTATCCCCTGATTCTGTGGATAACCGTAT
TACCGCCTTTGAGTGAGCTGATACCGCTCGCCGCAGCCGAACGACCGAGCGCAGCGAGTCAGTGA
GCGAGGAAGCGGAAGAGCGCCTGATGCGGTATTTTCTCCTTACGCATCTGTGCGGTATTTCACACC
GCATATATGGTGCACTCTCAGTACAATCTGCTCTGATGCCGCATAGTTAAGCCAGTATACACTCCG
CTATCGCTACGTGACTGGGTCATGGCTGCGCCCCGACACCCGCCAACACCCGCTGACGCGCCCTG
ACGGGCTTGTCTGCTCCCGGCATCCGCTTACAGACAAGCTGTGACCGTCTCCGGGAGCTGCATGTG
TCAGAGGTTTTCACCGTCATCACCGAAACGCGCGAGGCAGCTGCGGTAAAGCTCATCAGCGTGGT
CGTGAAGCGATTCACAGATGTCTGCCTGTTCATCCGCGTCCAGCTCGTTGAGTTTCTCCAGAAGCG
TTAATGTCTGGCTTCTGATAAAGCGGGCCATGTTAAGGGCGGTTTTTTCCTGTTTGGTCACTGATGC
CTCCGTGTAAGGGGGATTTCTGTTCATGGGGGTAATGATACCGATGAAACGAGAGAGGATGCTCA
CGATACGGGTTACTGATGATGAACATGCCCGGTTACTGGAACGTTGTGAGGGTAAACAACTGGCG
GTATGGATGCGGCGGGACCAGAGAAAAATCACTCAGGGTCAATGCCAGCGCTTCGTTAATACAGA
TGTAGGTGTTCCACAGGGTAGCCAGCAGCATCCTGCGATGCAGATCCGGAACATAATGGTGCAGG
GCGCTGACTTCCGCGTTTCCAGACTTTACGAAACACGGAAACCGAAGACCATTCATGTTGTTGCTC
AGGTCGCAGACGTTTTGCAGCAGCAGTCGCTTCACGTTCGCTCGCGTATCGGTGATTCATTCTGCT
AACCAGTAAGGCAACCCCGCCAGCCTAGCCGGGTCCTCAACGACAGGAGCACGATCATGCGCACCC
CGTGGGGCCGCCATGCCGGCGATAATGGCCTGCTTCTCGCCGAAACGTTTGGTGGCGGGACCAGT
GACGAAGGCTTGAGCGAGGGCGTGCAAGATTCCGAATACCGCAAGCGACAGGCCGATCATCGTC
GCGCTCCAGCGAAAGCGGTCCTCGCCGAAAATGACCCAGAGCGCTGCCGGCACCTGTCCTACGAG
TTGCATGATAAAGAAGACAGTCATAAGTGCGGCGACGATAGTCATGCCCCGCGCCCACCGGAAGG
AGCTGACTGGGTTGAAGGCTCTCAAGGGCATCGGTCGAGATCCCGGTGCCTAATGAGTGAGCTAA
CTTACATTAATTGCGTTGCGCTCACTGCCCGCTTTCCAGTCGGGAAACCTGTCGTGCCAGCTGCATT
AATGAATCGGCCAACGCGCGGGGAGAGGCGGTTTGCGTATTGGGCGCCAGGGTGGTTTTTCTTTTC
ACCAGTGAGACGGGCAACAGCTGATTGCCCTTCACCGCCTGGCCCTGAGAGAGTTGCAGCAAGCG
GTCCACGCTGGTTTGCCCCAGCAGGCGAAAATCCTGTTTGATGGTGGTTAACGGCGGGATATAAC
ATGAGCTGTCTTCGGTATCGTCGTATCCCACTACCGAGATATCCGCACCAACGCGCAGCCCGGACT
CGGTAATGGCGCGCATTGCGCCCAGCGCCATCTGATCGTTGGCAACCAGCATCGCAGTGGGAACG
ATGCCCTCATTCAGCATTTGCATGGTTTGTTGAAAACCGGACATGGCACTCCAGTCGCCTTCCCGT
TCCGCTATCGGCTGAATTTGATTGCGAGTGAGATATTTATGCCAGCCAGCCAGACGCAGACGCGCC
GAGACAGAACTTAATGGGCCCGCTAACAGCGCGATTTGCTGGTGACCCAATGCGACCAGATGCTC
CACGCCCAGTCGCGTACCGTCTTCATGGGAGAAAATAATACTGTTGATGGGTGTCTGGTCAGAGA
CATCAAGAAATAACGCCGGAACATTAGTGCAGGCAGCTTCCACAGCAATGGCATCCTGGTCATCC
AGCGGATAGTTAATGATCAGCCCACTGACGCGTTGCGCGAGAAGATTGTGCACCGCCGCTTTACA
GGCTTCGACGCCGCTTCGTTCTACCATCGACACCACCACGCTGGCACCCAGTTGATCGGCGCGAGA
TTTAATCGCCGCGACAATTTGCGACGGCGCGTGCAGGGCCAGACTGGAGGTGGCAACGCCAATCA
GCAACGACTGTTTGCCCGCCAGTTGTTGTGCCACGCGGTTGGGAATGTAATTCAGCTCCGCCATCG
CCGCTTCCACTTTTTCCCGCGTTTTCGCAGAAACGTGGCTGGCCTGGTTCACCACGCGGGAAACGG
TCTGATAAGAGACACCGGCATACTCTGCGACATCGTATAACGTTACTGGTTTCACATTCACCACCC
TGAATTGACTCTCTTCCGGGCGCTATCATGCCATACCGCGAAAGGTTTTGCGCCATTCGATGGTGT
CCGGGATCTCGACGCTCTCCCTTATGCGACTCCTGCATTAGGAAGCAGCCCAGTAGTAGGTTGAGG
CCGTTGAGCACCGCCGCCGCAAGGAATGGTGCATGCAAGGAGATGGCGCCCAACAGTCCCCCGGC
CACGGGGCCTGCCACCATACCCACGCCGAAACAAGCGCTCATGAGCCCGAAGTGGCGAGCCCGAT
CTTCCCCATCGGTGATGTCGGCGATATAGGCGCCAGCAACCGCACCTGTGGCGCCGGTGATGCCG
GCCACGATGCGTCCGGCGTAGAGGATCGAGATCTCGATCCCGCGAAATTAATACGACTCACTATA

GGGGAATTGTGAGCGGATAACAATTCCCCTCTAGAAATAATTTTGTTTAACTTTAAGAAGGAGATA
TACCATGggcCatcatcatcatcatcatTCCCCTATACTAGGTTATTGGAAAATTAAGGGCCTTGTGCAACCCA
CTCGACTTCTTTTGGAATATCTTGAAGAAAAATATGAAGAGCATTTGTATGAGCGCGATGAAGGTG
ATAAATGGCGAAACAAAAAGTTTGAATTGGGTTTGGAGTTTCCCAATCTTCCTTATTATATTGATG
GTGATGTTAAATTAACACAGTCTATGGCCATCATACGTTATATAGCTGACAAGCACAACATGTTGG
GTGGTTGTCCAAAAGAGCGTGCAGAGATTTCAATGCTTGAAGGAGCGGTTTTGGATATTAGATAC
GGTGTTTCGAGAATTGCATATAGTAAAGACTTTGAAACTCTCAAAGTTGATTTTCTTAGCAAGCTA
CCTGAAATGCTGAAAATGTTCGAAGATCGTTTATGTCATAAAACATATTTAAATGGTGATCATGTA
ACCCATCCTGACTTCATGTTGTATGACGCTCTTGATGTTGTTTTATACATGGACCCAATGTGCCTGG
ATGCGTTCCCAAAATTAGTTTGTTTTAAAAAACGTATTGAAGCTATCCCACAAATTGATAAGTACT
TGAAATCCAGCAAGTATATAGCATGGCCTTTGCAGGGCTGGCAAGCCACGTTTGGTGGTGGCGAC
CATCCTCCAAAAGAAAACCTGTATTTTCAGGGCCATATGTCATCAGAGGCTCGTATGTTCACCATT
TCGGATACCACGATGAAAGAAATTGATCGATTTCGTTTGCGGTTGAAGAAATCAGTTATGTATGCT
TTCATTCTCAAGGTTGATAAAGCTACTAAGGAGATTGTTCCCGATGGAGAAATCATGGATTTACAG
AGTATTGAAGAGGTCGCAGATGAACTCTCGGAAACAAATCCTAGATTTATCCTTGTTTCCTATCCT
ACCAAAACCACAGATGGTCGACTTAGTACTCCATTGTTTATGATATACTGGAGACCAAGTGCTACC
CCAAATGACTTATCTATGATTTATGCTTCTGCTAAAGTCTGGTTTCAAGATGTGTCGCAGGTGCAC
AAAGTATTTGAAGCTAGAGATTCTGAAGATATTACTAGTGAAGCAGTTGATGAGTTTTTGCATaagtg
taagTAAGAATTCGAGCTCCGTCGACAAGCTTGCGGCCGCACTCGAGCACCACCACCACCACCACTG
AGATCCGGCTGCTAACAAAGCCCGAAAGGAAGCTGAGTTGGCTGCTGCCACCGCTGAGCAATAAC
TAGCATAACCCCTTGGGGCCTCTAAACGGGTCTTGAGGGGTTTTTTGCTGAAAGGAGGAACTATAT
CCGGATTGGCGAATGGGACGCGCCCTGTAGCGGCGCATTAAGCGCGGCGGGTGTGGTGGTTACGC
GCAGCGTGACCGCTACACTTGCCAGCGCCCTAGCGCCCGCTCCTTTCGCTTTCTTCCCTTCCTTTCT
CGCCACGTTCGCCGGCTTTCCCCGTCAAGCTCTAAATCGGGGGCTCCCTTTAGGGTTCCGATTTAG
TGCTTTACGGCACCTCGACCCCAAAAAACTTGATTAGGGTGATGGTTCACGTAGTGGGCCATCGCC
CTGATAGACGGTTTTTCGCCCTTTGACGTTGGAGTCCACGTTCTTTAATAGTGGACTCTTGTTCCAA
ACTGGAACAACACTCAACCCTATCTCGGTCTATTCTTTTGATTTATAAGGGATTTTGCCGATTTCGG
CCTATTGGTTAAAAAATGAGCTGATTTAACAAAAATTTAACGCGAATTTTAACAAAATATTAACGT
TTACAATTTCAGGTGGCACTTTTCGGGGAAATGTGCGCGGAACCCCTATTTGTTTATTTTTCTAAAT
ACATTCAAATATGTATCCGCTCATGAATTAATTCTTAGAAAAACTCATCGAGCATCAAATGAAACT
GCAATTTATTCATATCAGGATTATCAATACCATATTTTTGAAAAAGCCGTTTCTGTAATGAAGGAG
AAAACTCACCGAGGCAGTTCCATAGGATGGCAAGATCCTGGTATCGGTCTGCGATTCCGACTCGTC
CAACATCAATACAACCTATTAATTTCCCCTCGTCAAAAATAAGGTTATCAAGTGAGAAATCACCAT
GAGTGACGACTGAATCCGGTGAGAATGGCAAAAGTTTATGCATTTCTTTCCAGACTTGTTCAACAG
GCCAGCCATTACGCTCGTCATCAAAATCACTCGCATCAACCAAACCGTTATTCATTCGTGATTGCG
CCTGAGCGAGACGAAATACGCGATCGCTGTTAAAAGGACAATTACAAACAGGAATCGAATGCAA
CCGGCGCAGGAACACTGCCAGCGCATCAACAATATTTTCACCTGAATCAGGATATTCTTCTAATAC
CTGGAATGCTGTTTTCCCGGGGATCGCAGTGGTGAGTAACCATGCATCATCAGGAGTACGGATAA
AATGCTTGATGGTCGGAAGAGGCATAAATTCCGTCAGCCAGTTTAGTCTGACCATCTCATCTGTAA
CATCATTGGCAACGCTACCTTTGCCATGTTTCAGAAACAACTCTGGCGCATCGGGCTTCCCATACA
ATCGATAGATTGTCGCACCTGATTGCCCGACATTATCGCGAGCCCATTTATACCCATATAAATCAG
CATCCATGTTGGAATTTAATCGCGGCCTAGAGCAAGACGTTTCCCGTTGAATATGGCTCATAACAC
CCCTTGTATTACTGTTTATGTAAGCAGACAGTTTTATTGTTCATGACCAAAATCCCTTAACGTGAGT
TTTCGTTCCACTGAGCGTCAGACCCCGTAGAAAAGATCAAAGGATCTTCTTGAGATCCTTTTTTTCT
GCGCGTAATCTGCTGC

References

1. J. A. Cooper, S. B. Walker, T. D. Pollard, Pyrene actin: documentation of the validity of a sensitive assay for actin polymerization. *J Muscle Res Cell Motil* **4**, 253-262 (1983).
2. M. F. Carlier, D. Pantaloni, Binding of Phosphate to F-Adp-Actin and Role of F-Adp-Pi-Actin in Atp-Actin Polymerization. *Journal of Biological Chemistry* **263**, 817-825 (1988).
3. M. F. Carlier, D. Pantaloni, Direct evidence for ADP-Pi-F-actin as the major intermediate in ATP-actin polymerization. Rate of dissociation of Pi from actin filaments. *Biochemistry* **25**, 7789-7792 (1986).
4. M. J. Dayel, R. D. Mullins, Activation of Arp2/3 complex: addition of the first subunit of the new filament by a WASP protein triggers rapid ATP hydrolysis on Arp2. *PLoS Biol* **2**, E91 (2004).
5. C. Le Clainche, D. Pantaloni, M. F. Carlier, ATP hydrolysis on actin-related protein 2/3 complex causes debranching of dendritic actin arrays. *Proc Natl Acad Sci U S A* **100**, 6337-6342 (2003).
6. B. A. Smith, K. Daugherty-Clarke, B. L. Goode, J. Gelles, Pathway of actin filament branch formation by Arp2/3 complex revealed by single-molecule imaging. *Proc Natl Acad Sci U S A* **110**, 1285-1290 (2013).
7. T. D. Pollard, A. G. Weeds, The rate constant for ATP hydrolysis by polymerized actin. *FEBS Lett* **170**, 94-98 (1984).
8. E. Atilgan, D. Wirtz, S. X. Sun, Morphology of the lamellipodium and organization of actin filaments at the leading edge of crawling cells. *Biophys J* **89**, 3589-3602 (2005).
9. M. Vinzenz *et al.*, Actin branching in the initiation and maintenance of lamellipodia. *J Cell Sci* **125**, 2775-2785 (2012).
10. G. L. Ryan, H. M. Petroccia, N. Watanabe, D. Vavylonis, Excitable actin dynamics in lamellipodial protrusion and retraction. *Biophys J* **102**, 1493-1502 (2012).
11. L. M. McMillen, D. Vavylonis, Model of turnover kinetics in the lamellipodium: implications of slow- and fast-diffusing capping protein and Arp2/3 complex. *Phys Biol* **13**, 066009 (2016).
12. T. Miyoshi *et al.*, Actin turnover-dependent fast dissociation of capping protein in the dendritic nucleation actin network: evidence of frequent filament severing. *J Cell Biol* **175**, 947-955 (2006).